LBL-2263
c.2

RELATION OF PROCESSING PARAMETERS TO THE PROPERTIES OF LITHIUM FERRITE

Gautam Bandyopadhyay
(Ph. D. thesis)

November 1973

Prepared for the U. S. Atomic Energy Commission
under Contract W-7405-ENG-48

TWO-WEEK LOAN COPY

This is a Library Circulating Copy which may be borrowed for two weeks. For a personal retention copy, call Tech. Info. Division, Ext. 5545

LAWRENCE BERKELEY LABORATORY
UNIVERSITY OF CALIFORNIA
BERKELEY

LBL-2263
c.2

DISCLAIMER

This document was prepared as an account of work sponsored by the United States Government. While this document is believed to contain correct information, neither the United States Government nor any agency thereof, nor the Regents of the University of California, nor any of their employees, makes any warranty, express or implied, or assumes any legal responsibility for the accuracy, completeness, or usefulness of any information, apparatus, product, or process disclosed, or represents that its use would not infringe privately owned rights. Reference herein to any specific commercial product, process, or service by its trade name, trademark, manufacturer, or otherwise, does not necessarily constitute or imply its endorsement, recommendation, or favoring by the United States Government or any agency thereof, or the Regents of the University of California. The views and opinions of authors expressed herein do not necessarily state or reflect those of the United States Government or any agency thereof or the Regents of the University of California.

RELATION OF PROCESSING PARAMETERS TO THE PROPERTIES OF LITHIUM FERRITE

Contents

ABSTRACT v

I. GENERAL INTRODUCTION 1

II. THERMOGRAVIMETRY OF SPINEL FERRITES 3

A. Introduction 3

B. Experimental Procedure 6
(1) Powder Preparation 6
(2) Thermogravimetric Analysis 7

C. Results and Discussion 8
(1) Weight Loss Run at Constant Heating Rate 8
(2) Equilibrated Weight Loss Run for the System $LiFeO_2$-$LiFe_5O_8$-Fe_2O_3 8
(3) Comparison of Weight Loss Behavior Amongst Various Ferrites 17

III. LITHIUM FERRITE - PROCESSING AND PROPERTIES 28

A. Introduction 28

B. Experimental Procedure 29
(1) Powder and Specimen Preparation 29
(2) Sintering Conditions 30
(3) Property Measurement 30

C. Results and Discussion 32
(1) Isothermal Sintering 32
(2) Nonstoichiometry and Its Relation to Densification and Microstructure 35
(3) X-ray Results 39
(4) DC Resistivity 43
(5) B-H Loop Parameters 51

IV. EFFECT OF DOPANTS 55

A. Introduction 55
B. Experimental Procedure 56
C. Results and Discussion 57
(1) Densification and Microstructure 57
(2) DC Resistivity 65
(3) B-H Loop Parameters 68

V. SUMMARY AND CONCLUSIONS 71

ACKNOWLEDGMENT 73

REFERENCES 74

RELATION OF PROCESSING PARAMETERS TO THE PROPERTIES OF LITHIUM FERRITE

Gautam Bandyopadhyay

Inorganic Materials Research Division, Lawrence Berkeley Laboratory
and Department of Materials Science and Engineering,
College of Engineering; University of California,
Berkeley, California 94720

ABSTRACT

Lithium ferrite spinel ($LiFe_5O_8$) and related compositions were investigated to characterize the lithium and oxygen loss during heat treatment, and also to determine the influence of sintering parameters, stoichiometry and selected dopants on the densification, microstructure and electrical and magnetic properties of the sintered material.

Extensive thermogravimetric work in air was done on the system $LiFeO_2$-$LiFe_5O_8$-Fe_2O_3. Both lithium and oxygen loss were considered. The weight loss data for other ferrites were compared with that of the lithium ferrite system and the influence of the cation distribution on the weight loss kinetics was demonstrated.

Cold pressed polycrystalline compacts of lithium ferrite with varying stoichiometry were sintered using a packing powder technique and 1 atm oxygen atmosphere to control the material loss from the system. These specimens were used to study the influence of sintering time and temperature, and stoichiometry on the densification, microstructural characteristics, dc resistivity and hysteresis loop parameters of lithium ferrite. The influence of packing powder composition was also investigated. It has been shown that the anion deficient compositions led to denser specimens with higher dc resistivity values and squarer B-H loops

having low coercive forces. But discontinuous grain growth was favored in these compositions.

The influence of controlled amounts of NiO and $NiFe_2O_4$ dopants on the processing and properties of lithium ferrite was also investigated. Densification was affected slightly by either of the dopants. NiO favored discontinuous grain growth, whereas $NiFe_2O_4$ suppressed it. Data were also presented relating dc resistivity and hysteresis loop parameters with the amount of dopants. The results were discussed in terms of compositional defects and microstructure.

I. GENERAL INTRODUCTION

Lithium ferrite ($LiFe_5O_8$) is one member of the series of compounds called "ferrites". It is ferrimagnetic and has an inverse spinel structure based on a face centered cubic packing of oxygens. Its chemical formula is $Fe^{+3}_{1.0}$ $[Li^{+1}_{0.5}$ $Fe^{+3}_{1.5}]$ O^{-2}_4, where the cations within the bracket are in the octahedral sites and those outside occupy the tetrahedral sites. Braun[1] first reported that a 1:3 order exists in the octahedral positions in lithium ferrite below approximately 750°C. Every row of octahedral ions in the [110] direction contains a lithium ion in every fourth site. Every Li^{+1} ion is surrounded by six Fe^{+3} ions and every Fe^{+3} ion has two Li^{+1} and four Fe^{+3} ions as neighbors. Lithium ferrite has a significantly higher Curie temperature[2] than that of the other commonly used ferrite materials, and with proper processing, very good square loop magnetic properties can be obtained.[3-8]

Processing lithium ferrite is complicated due to the loss of both lithium and oxygen during sintering. Recently Ridgeley et al.[9] correctly pointed out that wide variation in the literature data, on the physical parameters of lithium ferrite, exists and most of it can probably be related to the lack of precise knowledge about the stoichiometry of the material.

Most ferrites have a tendency to lose oxygen at high temperature. Lithium ferrite loses both oxygen and lithium during the heat treatment and thus adds to the problem of processing. Until recently[9,10] this aspect has been largely ignored. The first part of this investigation used thermogravimetry in the system $LiFeO_2$-$LiFe_5O_8$-Fe_2O_3 to characterize the material loss. Both lithium and oxygen loss were considered.

Weight loss data for some other spinel ferrites were also considered for comparison purposes. The second part of this investigation dealt with the influence of processing parameters on various properties. Previous investigators controlled the oxygen atmosphere during the sintering process to control the oxygen loss from the system. Few attempts have been made to control the lithium loss. In this investigation, a packing powder technique, as has been used extensively for the processing of lead zirconate titanate ceramics,[11] was employed to control lithium loss from the system. In the third and final part of this study the effect of some selective dopants on the processing and properties of lithium ferrite was investigated.

II. THERMOGRAVIMETRY OF SPINEL FERRITES

A. Introduction

Quantitative thermogravimetric analysis has been used by Reinjnen[12-14] to study the solid state reactions and the phase equilibria in the system $MgO-FeO-Fe_2O_3$. He gave an extensive discussion on the defect structure of ferrites and the possible equilibria that may exist in this system at high temperatures. The basic idea in all the thermogravimetric work on ferrites is that the oxygen content in the spinel at any temperature depends on the oxygen content in the ambient atmosphere. With the loss of oxygen Fe^{+3} reduces to Fe^{+2}. Likewise, oxygen may be absorbed during cooling thereby converting some of the Fe^{+2} to Fe^{+3}. A quantitative knowledge of the weight change characteristics is desired because it has a strong influence on the defect structure which, in turn, influences the sinterability and magnetic properties of the sintered ferrite.

Reinjnen in one of his papers[14] considered the reaction,

$$Fe^{+3} + 1/2\ O^{-2} \rightleftarrows Fe^{+2} + 1/4\ O_2(g) \qquad (1)$$

and showed that this equilibria does not represent the actual weight loss during the heat treatment of magnesium ferrite, because at higher temperatures a log(K) vs 1/T plot deviated significantly from the straight line relationship (K is the equilibrium constant for the reaction and T is the temperature in degrees Kelvin). He modified reaction 1 and suggested the following equilibria from the reaction equation

$$9Fe_{8/3}\square_{1/3}O_4 \rightarrow 8Fe_3O_4 + 2O_2(g),$$

$$Fe^{+3} + 3/8V_c + 1/2\ O^{-2} \rightleftarrows Fe^{+2} + 1/4\ O_2(g) \qquad (2)$$

where V_c is a vacant cation site, on the assumption that the cations and cation vacancies have no preference for either octahedral or tetrahedral sites.[13] He also took into account the spinel composition and the cation distribution, but still he found that his model was not adequate to describe all the details of the solid-oxygen equilibria in ferrites.[13] In spite of this drawback, the inherent simplicity of reaction 2 makes it extremely useful in the data analysis of the cation deficient ferrites.

The typical weight loss behavior for a Fe_2O_3 excess spinel ferrite is shown in Fig. 1 which is basically the same figure with minor changes as was shown by Reinjnen.[13] It is assumed that oxygen is the only vaporizing species in these systems. Initially a two phase composition loses material to enter the single phase spinel region. Then reaction 2 continues to annihilate the excess cation vacancies so that the composition approaches the stoichiometric point (metal:oxygen = 3:4). Beyond that the composition becomes anion deficient by the continued loss of oxygen. With further increase of temperature, the weight loss increases sharply due to the reaction,

$$Fe_3O_4 \rightleftarrows 3FeO + 1/2\ O_2(g) \qquad (3)$$

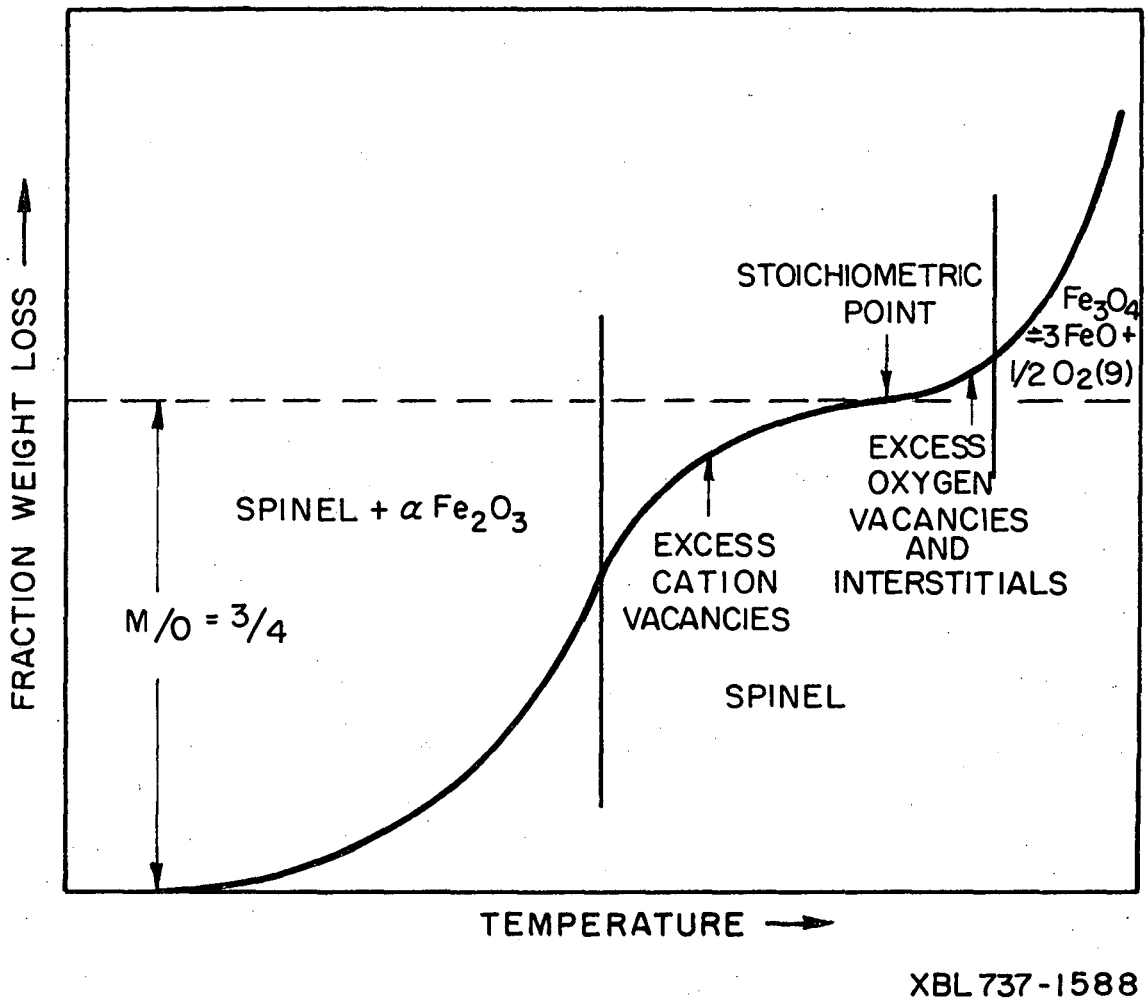

Fig. 1. Typical equilibrated weight loss behavior for a spinel ferrite with excess Fe_2O_3 (after Reinjnen[13]). It is assumed that oxygen is the only vaporizing species.

The experimental work done in this investigation is on the system $LiFeO_2$-$LiFe_5O_8$-Fe_2O_3, where oxygen as well as lithium loss is possible during the heat treatment. An attempt has been made to characterize the material loss behavior of this system in relation to the starting composition. The analysis has been extended to some other ferrites for comparison purposes.

B. Experimental Procedure

(1) Powder Preparation

All the powder preparation procedures were carefully optimized to get the best results.

For the preparation of stoichiometric lithium ferrite ($LiFe_5O_8$), suitable proportions of reagent grade Li_2CO_3 and Fe_2O_3 were mixed in a neoprene lined ball mill for 48 h using isopropyl alcohol and teflon balls as the mixing media. The alcohol was evaporated and the mixture was calcined at 800 C for 6 h in air. The powder was milled and was recalcined at 800 C for 8 h in 1 atm oxygen.

$LiFeO_2$ powder was also prepared in the identical way using suitable proportions of Li_2CO_3 and Fe_2O_3.

In order to make a series of powders with known deviation from the stoichiometric composition, $LiFe_5O_8$ was mixed with proper proportions of $LiFeO_2$ or Fe_2O_3 in a ball mill as described above for 24 h. Then the mixture was calcined at 800 C for 8 h in 1 atm oxygen.

$NiFe_2O_4$ and $ZnFe_2O_4$ compositions were prepared using NiO or ZnO and Fe_2O_3 as the starting material. The calcination temperature was 950 C for 5 h for $NiFe_2O_4$ and 850 C for 5 h for $ZnFe_2O_4$. The calcined powder was milled and was recalcined at 1000 C for 4 h in 1 atm oxygen.

X-ray diffraction for all of the above powders failed to detect any undesirable second phases in any of the compositions.

(2) Thermogravimetric Analysis

The weight loss experiments were conducted in air with the weight change recorded continuously. A platinum crucible containing the sample in fine powder form was suspended from a platinum wire which was connected to one arm of the microbalance into a kanthal wound tube furnace. A control thermocouple was kept at the hottest part of the furnace and the temperature was controlled by the use of a proportional controller. The accuracy of the equipment was about ±0.25 mgs which is somewhat low compared to that claimed by Reinjnen.[12,13] Therefore, in most of the experiments, a reasonably large quantity of powder (8gs) was used to compensate for the low sensitivity.

In all the runs the temperature was quickly brought to 700 C and was kept at that temperature for a sufficiently long time to reach equilibrium. The equilibrated weight at 700 C was always assumed as the original weight for the experiment.

(a) Constant heating rate runs. The temperature was raised at the rate of 3 C/min to 1150 C and then the furnace was cooled to 700 C. The weight loss was recorded continuously throughout the run. The weight that could not be regained by cooling to 700 C has been termed as the "irreversible weight loss".

(b) Equilibrated weight loss run. In these experiments equilibrium was achieved at each temperature by allowing the reactions to continue for sufficiently long time. In most of the cases the temperature was increased in the steps of 25 C from 700 C to 1225 C.

C. Results and Discussion

(1) Weight Loss Run at Constant Heating Rate

Weight loss in mgs/mole of powder has been plotted against temperature in Fig. 2 for various compositions which include pure $LiFeO_2$ to 20 mol% Fe_2O_3 in $LiFe_5O_8$. The data points for the 1, 3, 5 and 10 mol% Fe_2O_3 in $LiFe_5O_8$ (which are not shown in Fig. 2) fell within the lines for stoichiometric and 20 mol% Fe_2O_3 in $LiFe_5O_8$ compositions. The nature of the plots for stoichiometric and near stoichiometric powders was identical to Fig. 1. It must be noted that while the present data are for constant heating rate runs and equilibrium was never achieved, Fig. 1 was drawn by Reinjnen[13] on the basis of equilibrated runs. Thus Fig. 2 just describes the qualitative nature of the weight loss characteristics and their dependence on the starting composition. The increased weight loss at high temperature is most probably due to the lithia loss rather than due to the reaction 3, because 1050 C is somewhat low for reaction 3 to occur. Increased weight loss with increasing Fe_2O_3 content in the composition is attributed to the increased oxygen loss. This is evident from Fig. 3 which shows that this increased loss is almost entirely reversible.

(2) Equilibrated Weight Loss Run for the System $LiFeO_2$-$LiFe_5O_8$-Fe_2O_3

It is accepted that on heat treatment oxygen and lithium loss is possible from lithium ferrite compositions. The amount of loss would depend on the activity of the vaporizing species at the temperature of the experiment. In cases where Fe_2O_3 is in solid solution with spinel ferrites and oxygen is the only vaporizing species, reaction 2 should

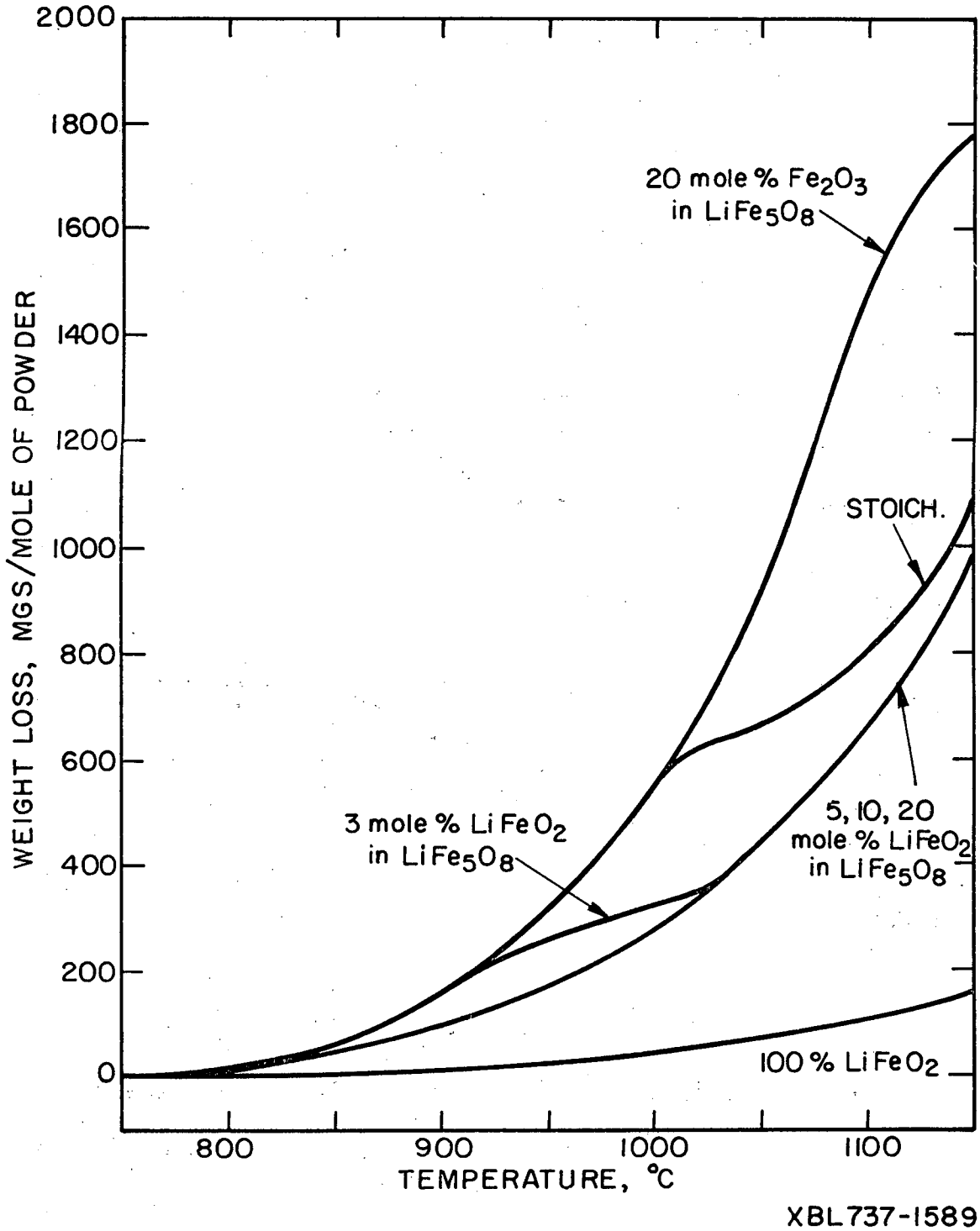

Fig. 2. Weight loss data for constant heating rate runs for various compositions in the system $LiFeO_2$-$LiFe_5O_8$-Fe_2O_3.

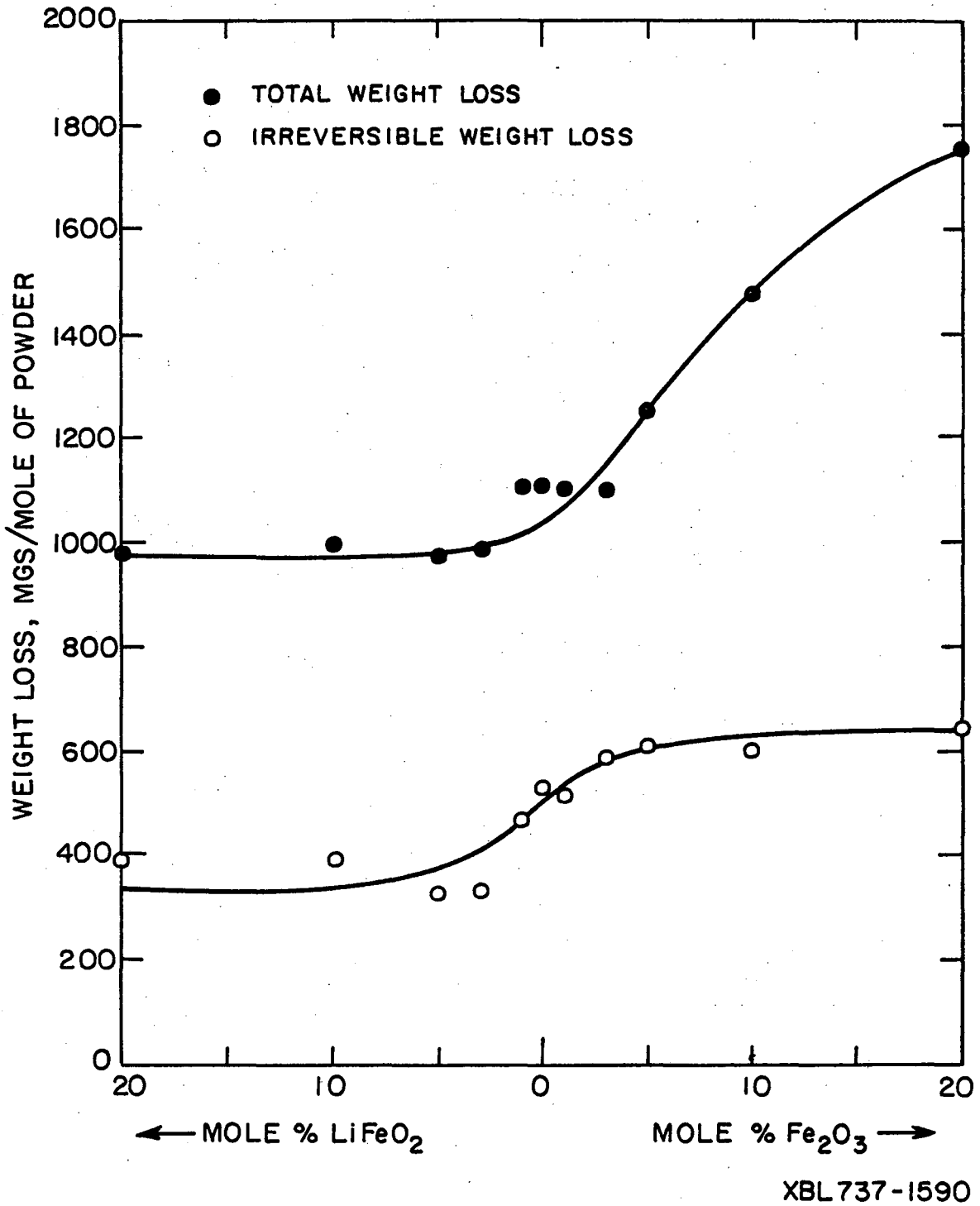

Fig. 3. Total weight loss and irreversible weight loss at 1150°C for various compositions. In each case the temperature was attained in a constant heating rate run.

describe the solid-oxygen equilibria as long as one remembers the limitations of this reaction. The equilibrium constant K for the reaction 2,

$$K = \frac{a_{O_2}^{1/4} \cdot [Fe^{+2}]}{[V_c]^{3/8}} \tag{4}$$

where $[O^{-2}]$ and $[Fe^{+3}]$ concentrations in the solid have been assumed unity. On rearrangement,

$$a_{O_2} = \left(\frac{K \cdot [V_c]^{3/8}}{[Fe^{+2}]} \right)^4 \tag{5}$$

Thus as the cation vacancy concentration decreases or Fe^{+2} concentration increases in the single phase composition, activity of oxygen decreases sharply. As the metal:oxygen (M:O) ratio approaches 3:4, the cation vacancy concentration drops to a low value. With further oxygen loss, oxygen vacancies may be created with excess cations in the interstitials. But a large deviation from the stoichiometry on the anion deficient side is not expected in the lithium ferrite system.[15] Thus the activity of oxygen would reach a constant value on the single phase boundary and would maintain that through the two phase region. Figure 4 schematically shows the change of oxygen activity with the change of the metal:oxygen ratio. In the same figure the expected variation of lithia activity is also shown. For simplicity it would be assumed that lithium is lost as Li_2O. The activity of lithia should reach a low value on the cation deficient single phase boundary region, as shown in Fig. 4.

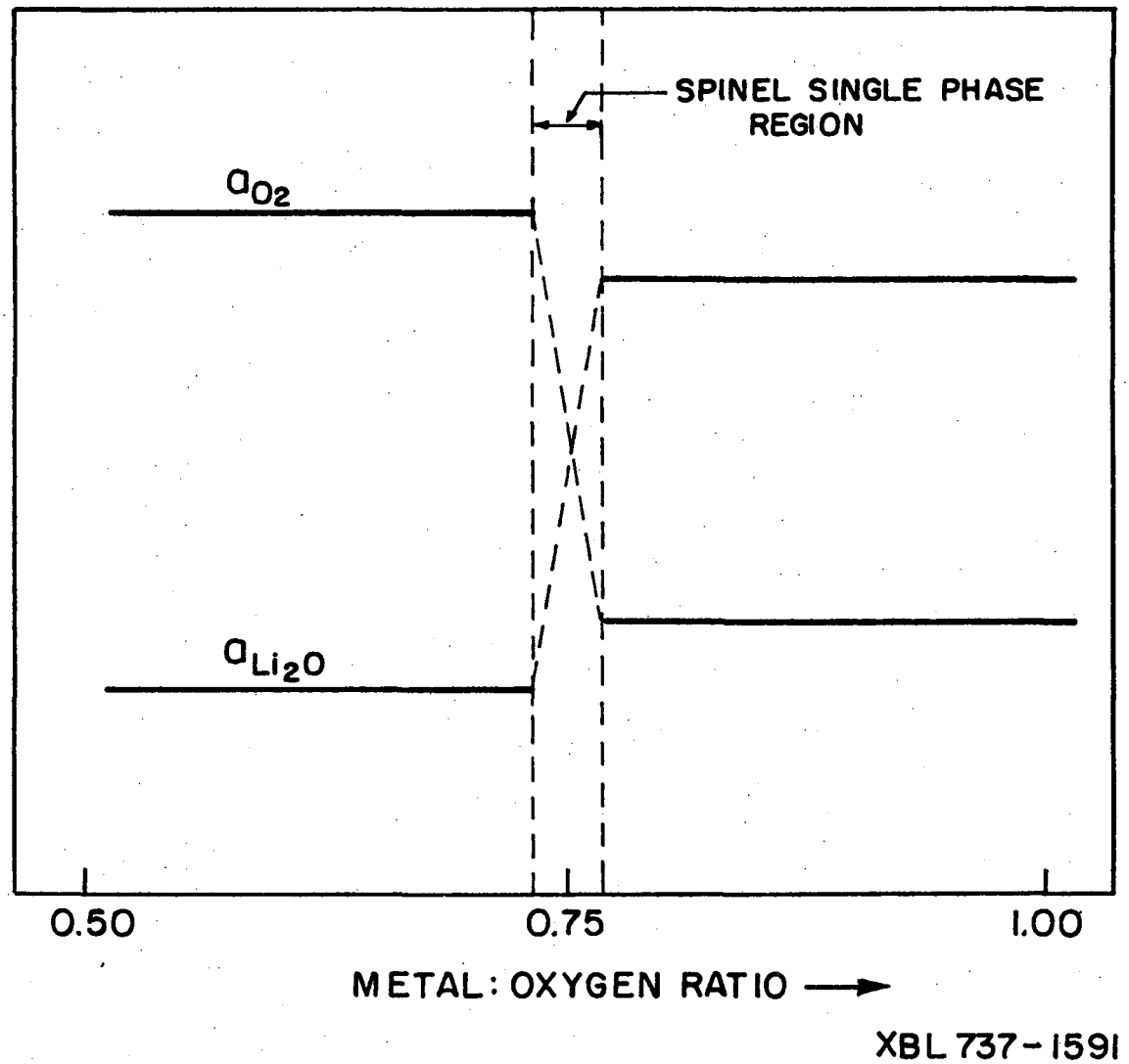

Fig. 4. Schematic representation of the variation of oxygen and lithia activity with respect to metal: oxygen ratio in the system $LiFeO_2$-$LiFe_5O_8$-Fe_2O_3.

The equilibrium condition in the thermogravimetric runs in air would be determined by reaction 2, where Eq. (4) can be written as,[12]

$$K = \frac{[Fe^{+2}]}{[V_c]^{3/8}} \cdot P_{O_2}^{1/4} \qquad (6)$$

where P_{O_2} is the partial pressure of oxygen in air. Since in most of the cases equilibrium was achieved, it is assumed that despite significant lithia loss from the lithium ferrite system, reaction 2 primarily controlled the equilibrium conditions.

Figure 5 shows the equilibrium weight loss behavior as a function of temperature for a lithium ferrite composition with 5 mol% excess Fe_2O_3. The nature of the plot is similar to that shown in Fig. 1. As is indicated, the two phase starting composition enters the single phase region followed by increasing weight loss at higher temperatures. The irreversible weight loss for the same run is also plotted in Fig. 5. It is interesting to note that in the middle portion of the curve, which is supposedly the single phase region, the irreversible weight loss remains practically constant. This indicates that lithium loss is insignificant in that region. It is also clear that the increasing weight loss at higher temperatures is at least partly due to the lithia loss as is indicated by the increased irreversible weight loss. In Fig. 6 log (Δg) for two lithium ferrite based compositions has been plotted against 1/T where Δg is the actual weight loss in mgs/mole of powder and T is the temperature in degrees Kelvin. The same data have been summarized in Table I. For the cation deficient composition ($LiFe_5O_8$ with excess Fe_2O_3) the single phase region is characterized by the more or

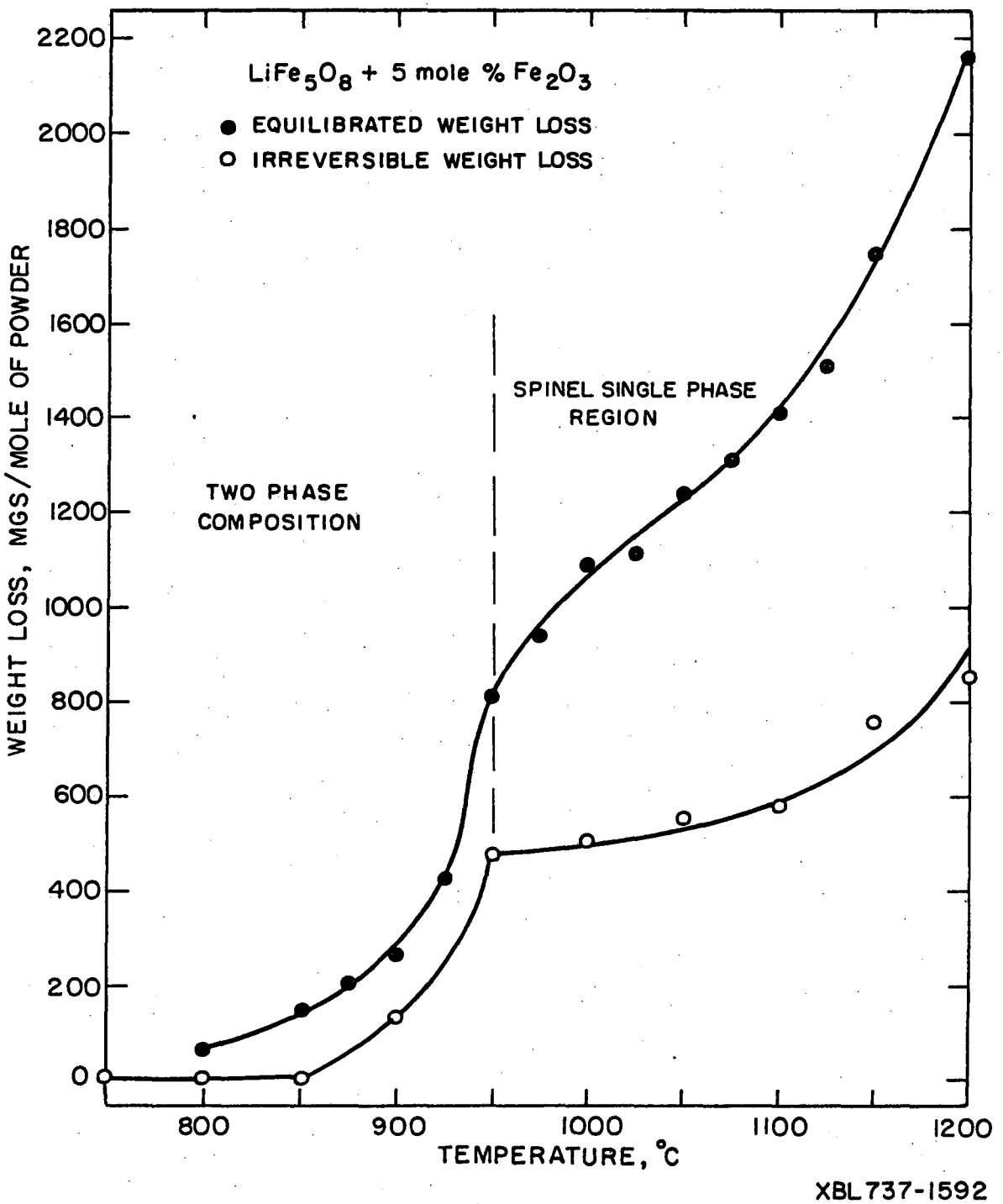

Fig. 5. Equilibrated and corresponding irreversible weight loss data for Fe_2O_3 excess $LiFe_5O_8$ composition.

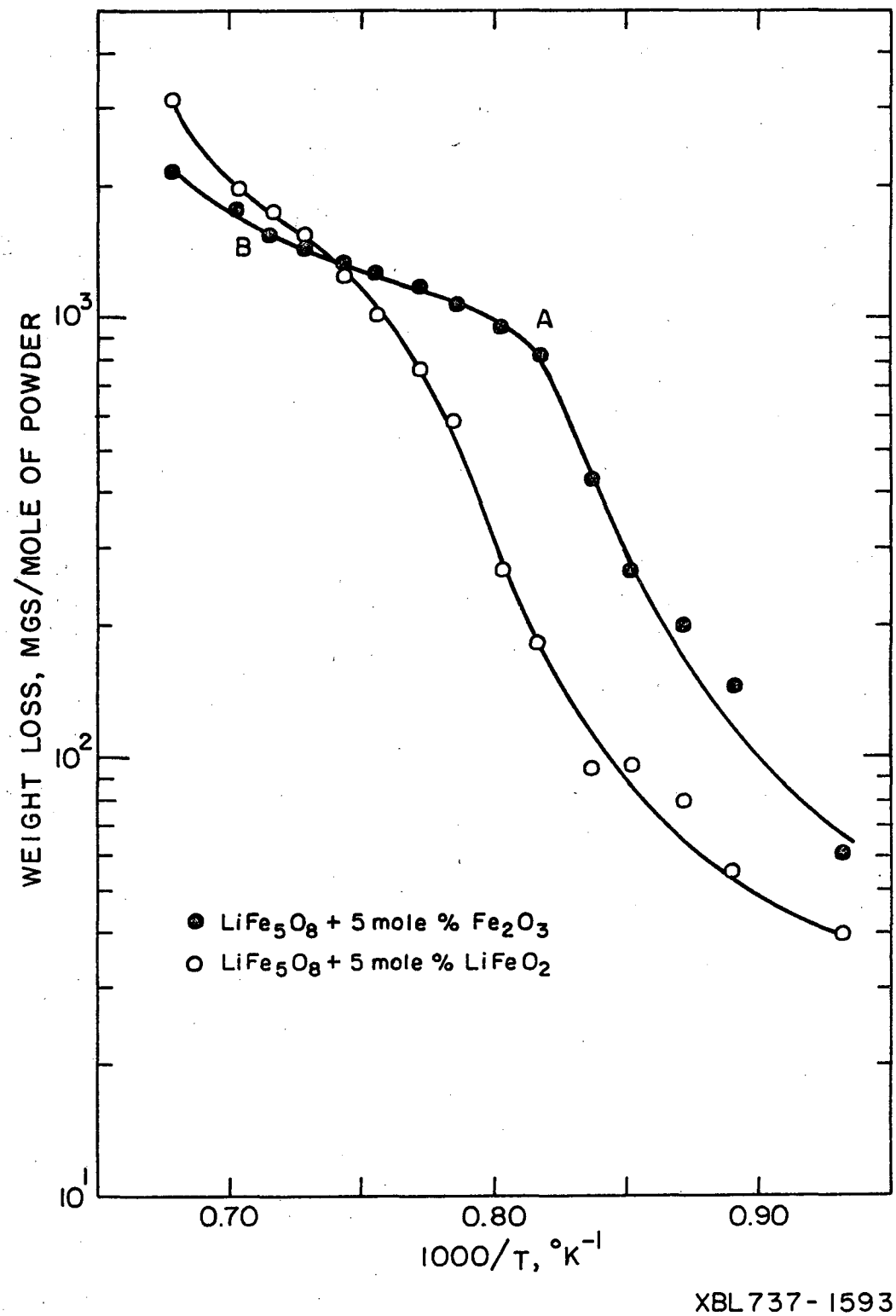

Fig. 6. Logarithm of weight loss/mole of powder (Δg) plotted against 1/T for equilibrated thermogravimetric runs using Fe_2O_3 excess and $LiFeO_2$ excess $LiFe_5O_8$.

Table I. Equilibrated weight loss data at various temperatures for Fe_2O_3 excess and $LiFeO_2$ excess lithium ferrite compositions

T °C	$\frac{10^3}{T}$ °K^{-1}	$LiFe_5O_8$ + 5 mol% Fe_2O_3 Δg mgs/mole	$LiFe_5O_8$ + 5 mol% $LiFeO_2$ Δg mgs/mole
700	1.0280	0.0	0.0
800	0.9320	6.06 x 10	2.38 x 10
850	0.8905	1.46×10^2	4.76 x 10
875	0.8715	2.02×10^2	7.94 x 10
900	0.8525	2.62×10^2	9.53 x 10
925	0.8360	4.29×10^2	9.53 x 10
950	0.8177	8.19×10^2	1.825×10^2
975	0.8035	9.35×10^2	2.62×10^2
1000	0.7855	1.086×10^3	3.18×10^2
1025	0.7720	1.17×10^3	7.6×10^2
1050	0.7559	1.24×10^3	1.015×10^3
1075	0.7430	1.31×10^3	1.24×10^3
1100	0.7283	1.41×10^3	1.53×10^3
1125	0.7153	1.51×10^3	1.73×10^3
1150	0.7027	1.74×10^3	1.98×10^3
1200	0.6780	2.16×10^3	3.12×10^3

less straight line portion of the curve (region AB). At higher temperatures lithia loss becomes significant and deviation from the straight line relationship occurs. For the lithia rich composition initial weight loss is significantly lower than that for the Fe_2O_3 rich composition. At one point excess lithia is lost and the composition enters the single phase region. Then lithia and oxygen loss continues simultaneously. Figure 7 schematically shows the compositional shift for the lithia rich (point a) and Fe_2O_3 rich (point b) starting materials and their path of entry (shown by dotted lines with arrows) to the single phase region.

(3) Comparison of Weight Loss Behavior Amongst Various Ferrites

Oxygen loss through reaction 2 is the primary weight loss mechanism in a cation deficient ferrite. But in the case of lithium ferrite, as we have already seen, significant lithium loss is possible along with the oxygen loss. In order to compare the weight loss behavior of lithium ferrite with that of other ferrites, it is necessary to select the region (e.g. the spinel single phase region in Fig. 5) where lithium loss is negligible compared to the oxygen loss. In this region it can be assumed, like in other ferrites, that only reaction 2 determines the weight loss. Using the simple approach used by Reinjnen,[12] at equilibrium one can write for reaction 2,

$$\frac{\Delta g}{(\Delta g_m - \Delta g)^{3/8}} = K = A \cdot \exp(-Q/RT) \qquad (7)$$

where Δg is the actual weight loss in mgs/mole of powder, Δg_m is the amount of oxygen to be lost per mole of powder to annihilate all the

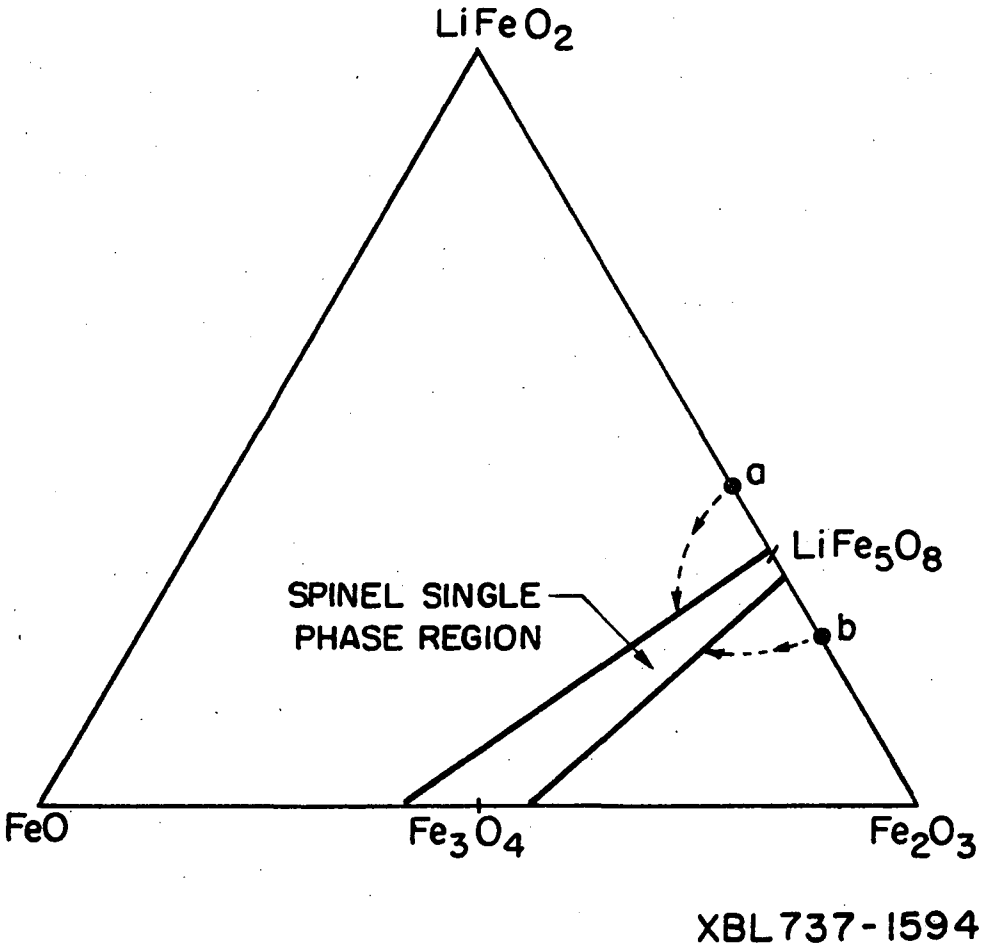

Fig. 7. Schematic representation of the path of entry of the two phase starting compositions into the single phase region.

excess cation vacancies in the system, A is a constant and Q is the activation energy for the reaction. Using this equation, Reinjnen[12] plotted

$$[\log\left(\frac{\Delta g}{\Delta g_m}\right) 10^2 - 3/8\cdot\log\left(1 - \frac{\Delta g}{\Delta g_m}\right) 10^2]$$

against 1/T for a cation deficient magnesium ferrite composition and then, from the slope of the straight line portion determined the activation energy for the reaction. In the case of lithium ferrite or zinc ferrite compositions, it is quite difficult to determine the Δg_m value because of the possibility of lithium or zinc loss at high temperature. Because, for a low Δg value log (Δg) vs 1/T relationship should approximate a straight line (according to Eq. (7)), comparisons can be made by internally normalizing Δg and 1/T values for each ferrite. The method of normalization can be described by the idealized log (Δg) vs 1/T plot (Fig. 8). It is to be noted that at higher temperatures deviation from the straight line relationship (as shown by the dotted line) is expected. The normalized Δg and 1/T values have been defined as,

$$(\Delta g)_{nor} = \left(\Delta g/\Delta g_A\right); \text{ and } (1/T)_{nor} = (1/T_A) - (1/T)$$

where Δg_A and T_A represent the weight loss and temperature respectively at the point A. Thus we see that only the single phase regions would be considered for comparison. In Fig. 9, log $(\Delta g)_{nor}$ values have been plotted against $(1/T)_{nor}$. The data are also recorded in Table II. It

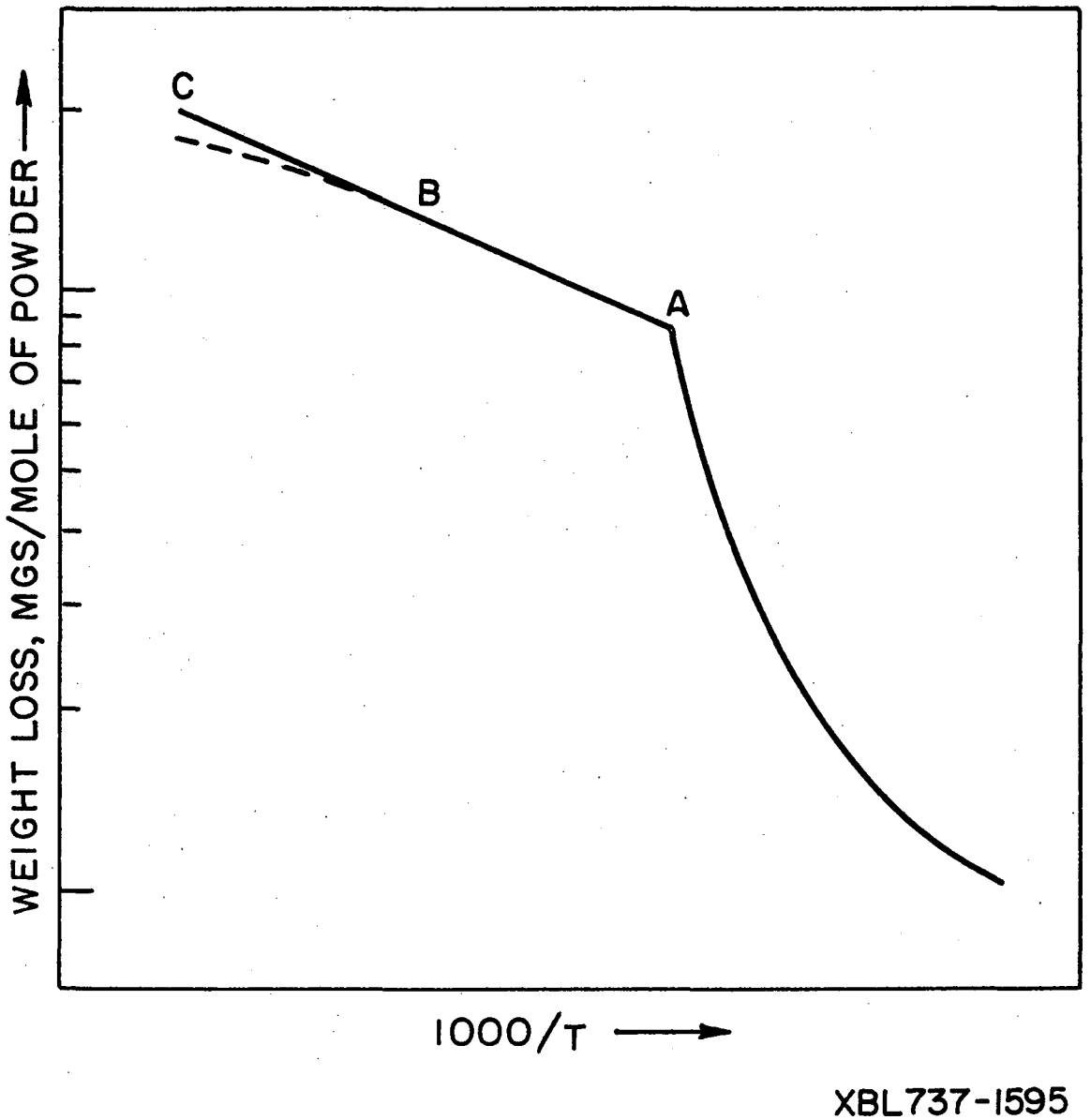

Fig. 8. Idealized log (weight loss) vs 1/T relationship.

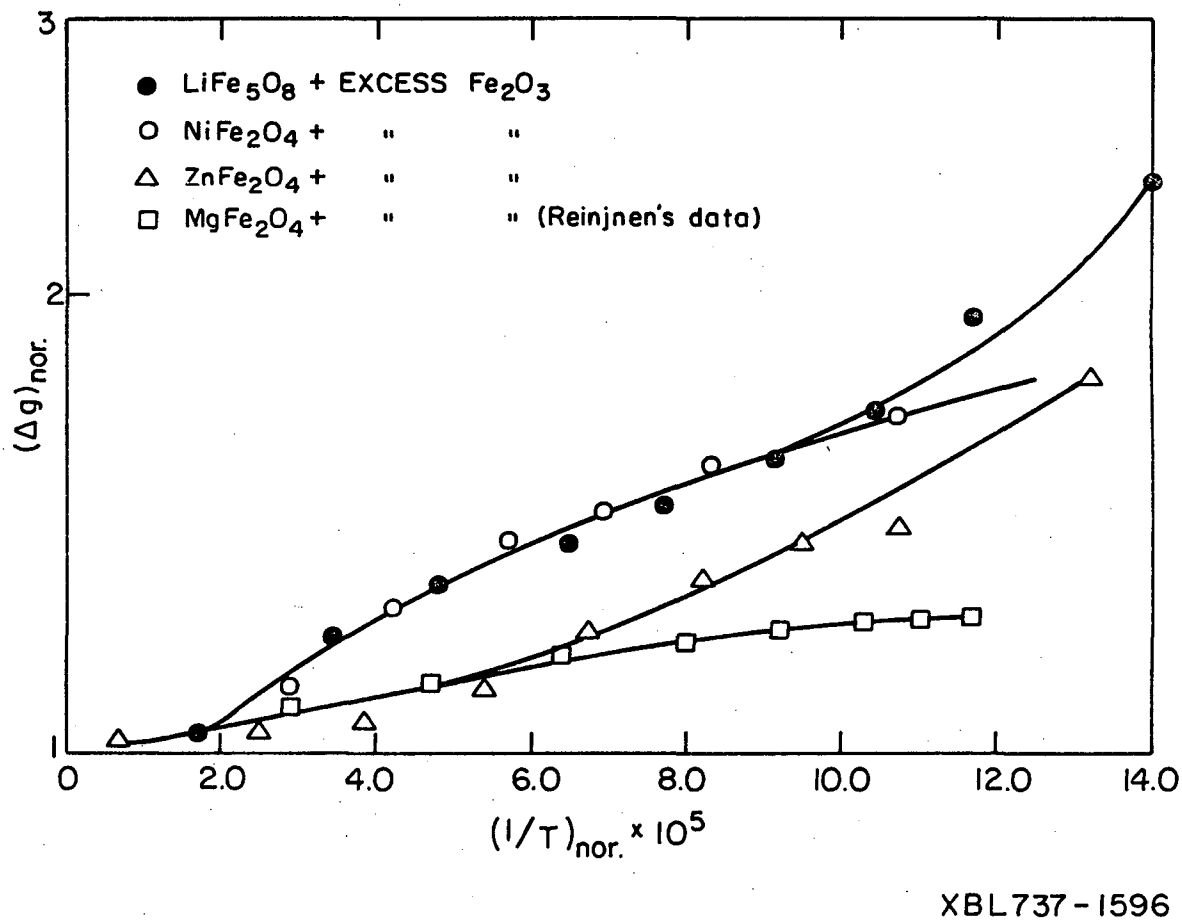

Fig. 9. Relationship between the normalized weight loss values $[(\Delta g)_{nor.}]$ and normalized 1/T for various Fe_2O_3 excess spinel ferrite compositions.

Table II. $(\Delta g)_{nor}$ and $(1/T)_{nor}$ values for different cation deficient spinel ferrites

Composition	Δg_A mgs/mole	$10^3/T_A$ $^oK^{-1}$	$10^3/T$ $^oK^{-1}$	$(1/T) \times 10^5$ nor	Δg mgs/mole	$(\Delta g)_{nor}$
$LiFe_5O_8$ + 5 mol% Fe_2O_3	0.91×10^3	0.82	0.82	0	0.91×10^3	1.000
			0.8035	1.65	0.935×10^3	1.028
			0.7855	3.45	1.086×10^3	1.190
			0.7720	4.80	1.17×10^3	1.288
			0.7559	6.41	1.24×10^3	1.363
			0.7430	7.70	1.31×10^3	1.440
			0.7283	9.17	1.41×10^3	1.550
			0.7153	10.47	1.51×10^3	1.660
			0.7027	11.73	1.74×10^3	1.910
			0.6780	14.20	2.16×10^3	2.380
$NiFe_2O_4$ + 5 mol% Fe_2O_3	0.42×10^3	0.785	0.785	0	4.20×10^2	1.0
			0.772	1.30	4.26×10^2	1.014
			0.7559	2.91	4.63×10^2	1.100
			0.7430	4.20	5.2×10^2	1.24
			0.7283	5.67	5.76×10^2	1.371
			0.7153	6.97	6.01×10^2	1.431
			0.7027	8.23	6.38×10^2	1.52
			0.678	10.7	6.93×10^2	1.65

Composition	Δg_A mgs/mole	$10^3/T_A$ $^oK^{-1}$	$10^3/T$ $^oK^{-1}$	$(1/T) \times 10^5$ nor	Δg mgs/mole	$(\Delta g)_{nor}$
$ZnFe_2O_4$ + 5 mol% Fe_2O_3	0.16×10^3	0.81	0.8100	0	1.60×10^2	1.000
			0.8035	0.0065	1.63×10^2	1.020
			0.7855	0.0245	1.655×10^2	1.030
			0.7720	0.0380	1.685×10^2	1.053
			0.7559	0.0541	1.775×10^2	1.110
			0.7430	0.0670	1.923×10^2	1.200
			0.7283	0.0817	2.070×10^2	1.294
			0.7153	0.0947	2.190×10^2	1.370
			0.7027	0.1073	2.250×10^2	1.400
			0.6780	0.1320	2.81×10^2	1.760

Composition	$\frac{\Delta g_A}{g} \times 10^4$	$10^3/T_A$ $^oK^{-1}$	$10^3/T$ $^oK^{-1}$	$(1/T) \times 10^5$ nor	$\frac{\Delta g}{g}^* \times 10^4$	$(\Delta g)_{nor}$
$MgFe_2O_4$ + excess Fe_2O_3 (Reinjnen's data[12])	50.0	0.725	0.725	0	-	-
			0.696	0.029	52.60	1.052
			0.678	0.047	55.70	1.114
			0.661	0.064	57.95	1.159
			0.645	0.080	59.30	1.186
			0.633	0.092	60.05	1.201
			0.622	0.103	60.60	1.212
			0.615	0.110	61.05	1.231
			0.608	0.117	61.30	1.226

* $\frac{\Delta g}{g}$ values were adjusted according to the assumption that 700°C is the start of the experiment. Thus $(\frac{\Delta g}{g})_{Adj} = (\frac{\Delta g}{g})_{actual} - (\frac{\Delta g}{g})_{700°}$ $[(\frac{\Delta g}{g})_{700} = 2.5]$.

is interesting to note that the inverse spinel compositions ($LiFe_5O_8$ or $NiFe_2O_4$) show different behavior than that shown by $ZnFe_2O_4$ or $MgFe_2O_4$. $ZnFe_2O_4$ is a normal spinel and $MgFe_2O_4$ has cation distribution very close to normal spinel. The increased weight loss at high temperature for lithium ferrite and zinc ferrite compositions is probably due to lithium and zinc loss respectively. Thus from the above discussion we see that, despite the crude approach, Fig. 9 distinctly points out the influence of cation distribution on the weight loss behavior in a cation deficient single phase ferrite.

For a further comparison

$$[\log \left(\frac{\Delta g}{\Delta g_m}\right) \cdot 10^2 - 3/8 \log \left(1 - \frac{\Delta g}{\Delta g_m}\right) \cdot 10^2]$$

values for the cation deficient nickel ferrite composition have been plotted against 1/T in Fig. 10. As has been mentioned earlier, the same plot for lithium ferrite or zinc ferrite compositions could not be drawn because of the difficulty in determining the Δg_m value due to lithium or zinc loss. As was noted by Reinjnen[12] for a magnesium ferrite composition, a straight line relationship has been obtained in the single phase region of the cation deficient nickel ferrite. The points in the single phase region have been normalized with respect to the point "X" and have been replotted in Fig. 11 (also summarized in Table III), along with the data for magnesium ferrite.[12] As expected, the nickel ferrite composition exhibited a different activation energy (32.75 kcal/mol) for reaction 2 than that exhibited by $MgFe_2O_4$ (22.8 kcal/mol).[12]

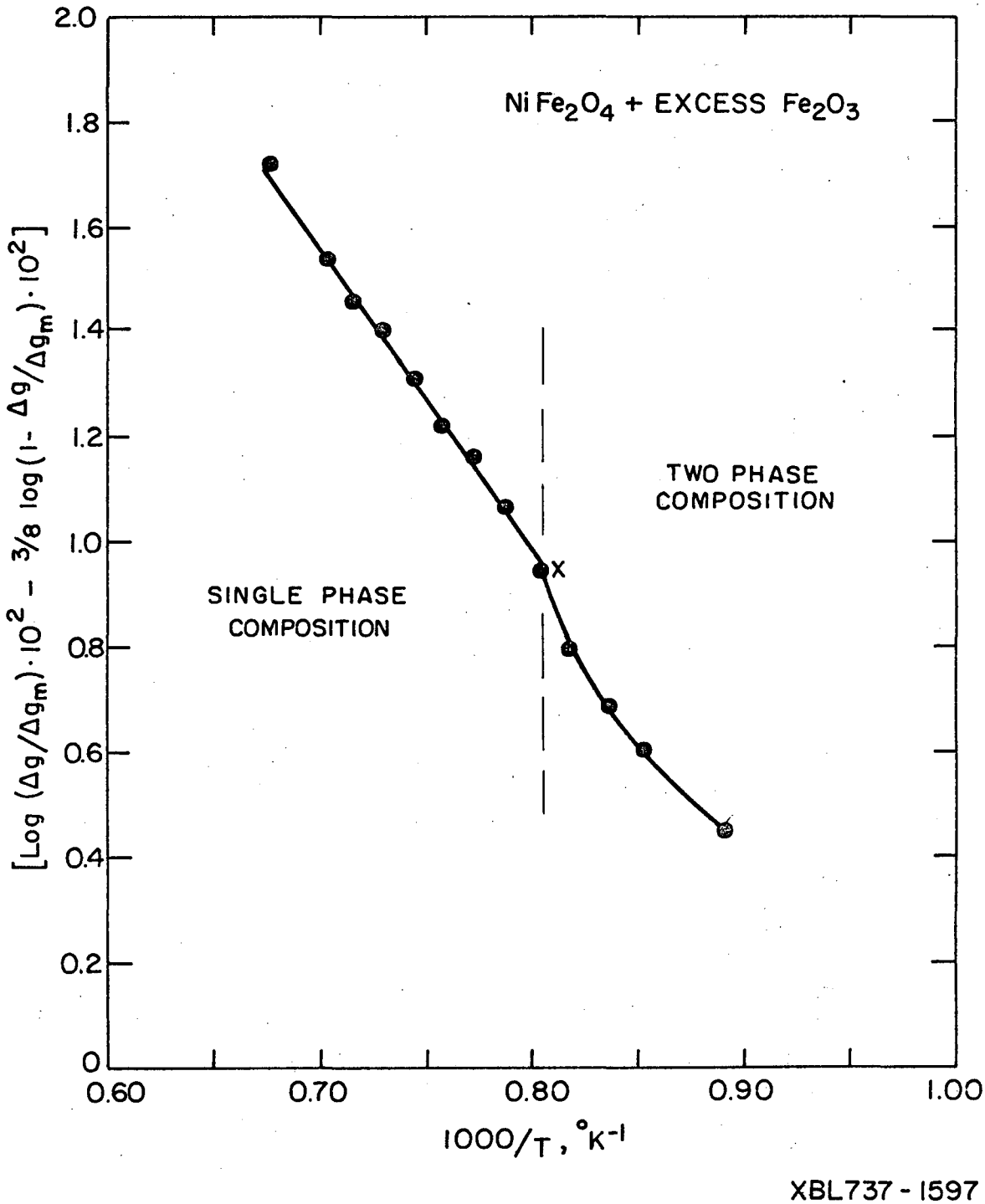

Fig. 10. $[\mathrm{Log}\ (\Delta g/\Delta g_m)\cdot 10^2 - 3/8 \log (1 - \frac{\Delta g}{\Delta g_m})\cdot 10^2]$ vs 1/T relationship for Fe_2O_3 excess $NiFe_2O_4$ composition.

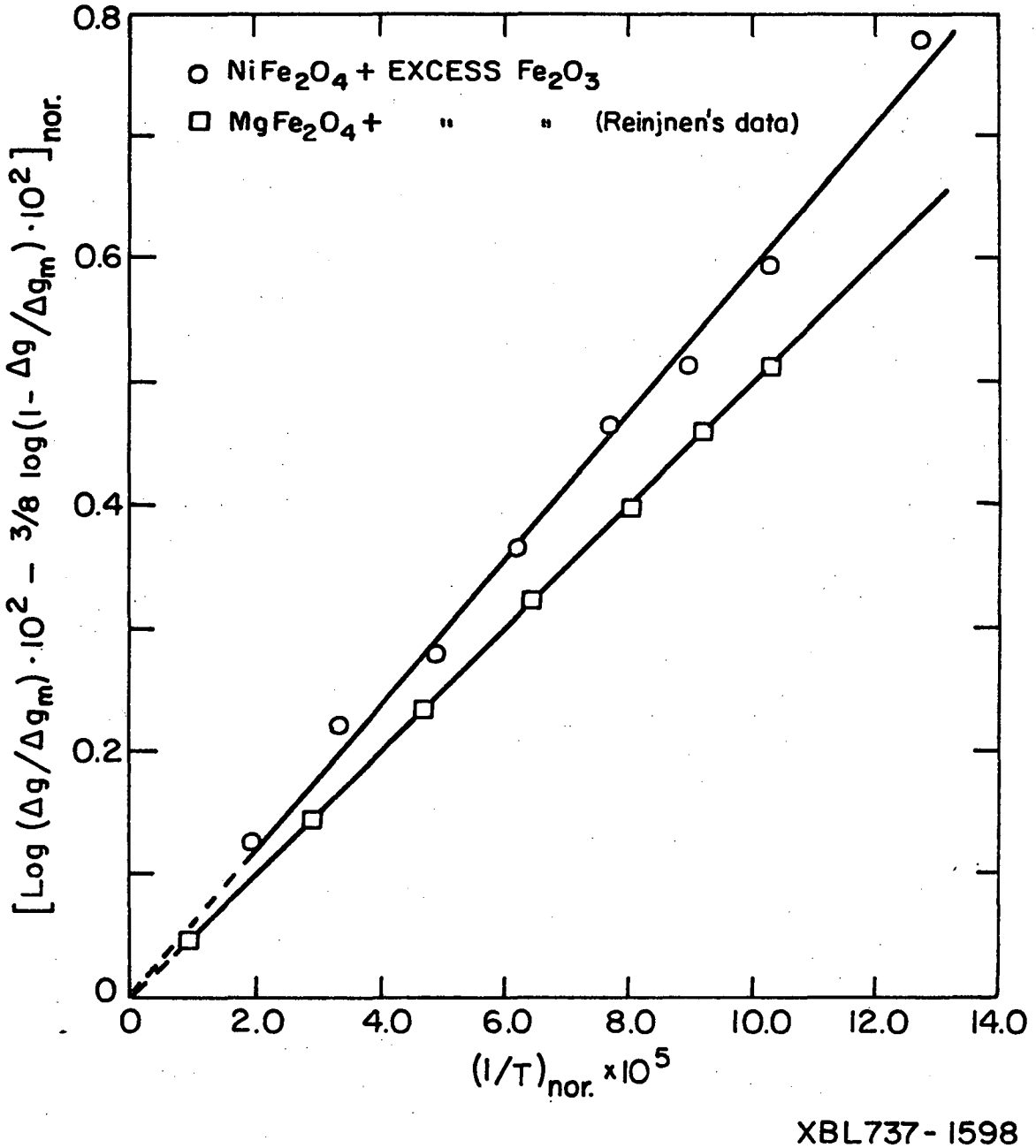

Fig. 11. Relationship between the normalized values of $[\mathrm{Log}\ (\Delta g/\Delta g_m)\cdot 10^2 - 3/8 \log\ (1 - \Delta g/\Delta g_m)\cdot 10^2]$ and 1/T for Fe_2O_3 excess $NiFe_2O_4$ and $MgFe_2O_4$ compositions. Activation energies calculated from the slope are 32.75 kcal/mol for $NiFe_2O_4$ and 22.8 kcal/mol for $MgFe_2O_4$.[12]

Table III. $[\mathrm{Log}\,(\frac{\Delta g}{\Delta g_m})\cdot 10^2 - 3/8 \log (1 - \frac{\Delta g}{\Delta g_m})\cdot 10^2]_{nor}$ and $(1/T)_{nor}$ values for two different cation deficient spinel ferrites

Composition	$10^3/T$ $^oK^{-1}$	$f(\Delta g,\Delta g_m)^*$	$(1/T)_{nor} \times 10^5$	$[f(\Delta g,\Delta g_m)]_{nor}$
$NiFe_2O_4$ + 5 mol%	0.9320	0.1761		
	0.8905	0.4464		
Fe_2O_3	0.8525	0.6095		
	0.8360	0.6859		
	0.8177	0.7968		
$[10^3/T_x = 0.805;$	0.8035	0.9366		
	0.7855	1.0630	1.95	0.1230
$f(\Delta g,\Delta g_m)_x = 0.94]$	0.7720	1.1593	3.30	0.2193
	0.7559	1.2158	4.91	0.2758
	0.7430	1.3052	6.20	0.3652
	0.7283	1.4018	7.67	0.4618
	0.7153	1.4503	8.97	0.5103
	0.7027	1.5307	10.23	0.5907
	0.6780	1.7156	12.70	0.7756
$MgFe_2O_4$ + excess	0.860	0.610		
	0.834	0.710		
Fe_2O_3	0.805	0.810		
	0.780	0.930		
(Reinjnen's data[12])	0.756	1.090		
	0.734	1.270		
$[10^3/T_x = 0.725;$	0.716	1.395	0.9	0.045
	0.696	1.493	2.9	0.143
$f(\Delta g,\Delta g_m)_x = 1.35]$	0.678	1.583	4.7	0.233
	0.661	1.670	6.4	0.320
	0.645	1.748	8.0	0.398
	0.633	1.808	9.2	0.458
	0.622	1.861	10.3	0.511
	0.615	1.928	11.0	0.578
	0.608	1.965	11.7	0.615

$* \; f(\Delta g,\Delta g_m) = [\log (\frac{\Delta g}{\Delta g_m})\cdot 10^2 - 3/8 \log (1 - \frac{\Delta g}{\Delta g_m})\cdot 10^2]$

$[f(\Delta g,\Delta g_m)]_{nor} = [\log (\frac{\Delta g}{\Delta g_m})\cdot 10^2 - 3/8 \log (1 - \frac{\Delta g}{\Delta g_m})\cdot 10^2]_{nor}$

$10^3/T_x = 10^3/T$ at the point x

$f(\Delta g,\Delta g_m)_x = f(\Delta g,\Delta g_m)$ at the point x.

III. LITHIUM FERRITE - PROCESSING AND PROPERTIES

A. Introduction

Processing of ceramic materials is an extremely involved subject in itself, and for any kind of reproducibility in the characteristics and properties of the final product, each of the processing steps must be evaluated carefully. Although considerable effort has been directed to understand the fundamentals of ceramic processing,[16] much of the existing knowledge is qualitative in nature. Most processing schemes have developed through programatic studies. The difficulties become obvious, when we count the number of variables that may be important in the system. The best way to study the effect of one or more known variables is to keep all other variables constant as far as possible. In this investigation, conventional ceramic methods, e.g., cold compaction followed by sintering have been used for the preparation of dense polycrystalline ferrites. A standard method of powder treatment and compaction procedure was used to keep the uncertainties to a minimum. Attempts were made to use powders from a single batch. The main emphasis in this section includes the study of the sintering step in relation to the time, temperature, atmosphere of sintering and nonstoichiometry, and their effects on the final properties of the dense lithium ferrite.

It is clear that a precise knowledge of the processing conditions is necessary to reach any conclusion. As was shown in the previous section, sintering of lithium ferrite may lead to a significant material loss unless proper precautions are taken. This type of material loss may introduce nonstoichiometry in the composition and in the extreme cases, second phases may appear. The nonstoichiometry in the ferrite

composition is known to have drastic influence on the densification behavior and on other properties. Thus it is essential to control the sintering conditions. A high O_2 atmosphere was used in most sintering runs to reduce oxygen loss, and lithium loss was controlled by the use of packing powders.

Amongst the various properties investigated, densification behavior and microstructure were characterized. DC resistivity values and hysteresis loop parameters were measured and were correlated with the sintering conditions and microstructure.

B. Experimental Procedure

(1) Powder and Specimen Preparation

The method of preparation of lithium ferrite and $LiFeO_2$ is identical to that described in the previous section except that the second calcination was eliminated for these powders. X-ray diffraction of lithium ferrite detected traces of $LiFeO_2$ and α-Fe_2O_3 in the composition. From now on this powder will be termed as "stoichiometric powder."

In order to make a series of powders with known deviations from the stoichiometric composition, $LiFe_5O_8$ was mixed with proper proportions of $LiFeO_2$ or Fe_2O_3 in a ball mill as described previously. The packing powders were prepared in the same way except that the last milling was eliminated to keep the particle size somewhat coarse.

Specimens, 1 in. diameter and 1/4 in. thick, were prepared by cold pressing at pressures less than 15,000 psi. Sample weight and size were controlled to give a constant density of all the specimens of approximately 53% of the theoretical value.

(2) Sintering Conditions

Isothermal sintering runs at 1 atm O_2 and using a stoichiometric packing powder were carried out at four different temperatures (1100°, 1150°, 1200°, 1250°C). Specimens were always buried deep into the packing powder and the same amount of packing powder was used in all the sintering runs.

In order to study the influence of nonstoichiometry on various properties, standard specimens of different starting compositions were sintered at 1150°C for 2 h in 1 atm O_2 and using stoichiometric packing powder. In some cases stoichiometric specimens were used and the packing powder composition was varied.

(3) Property Measurement

Density of the sintered specimens was measured by water displacement and also by geometric measurements. Theoretical density for the stoichiometric lithium ferrite composition was taken as 4.752 gs/cc. Corrections were made for any change in the starting composition.

For the microstructural investigation, specimens were polished and then thermally etched at 975°C for 15 min as suggested by West and Blankenship.[7] For some compositions, a longer time was necessary.

DC resistivity was measured by using a guard ring method (Fig. 12). Indium amalgam was used as the electrode material and standard sized specimens were used. Extremely reproducible data were obtained by using this method and it was possible to simultaneously measure the bulk and surface resistivity of a specimen.

Hysteresis loop parameters were measured from a B-H curve taken at 60 Hz using a torroidal shape specimen. The size of the specimens for

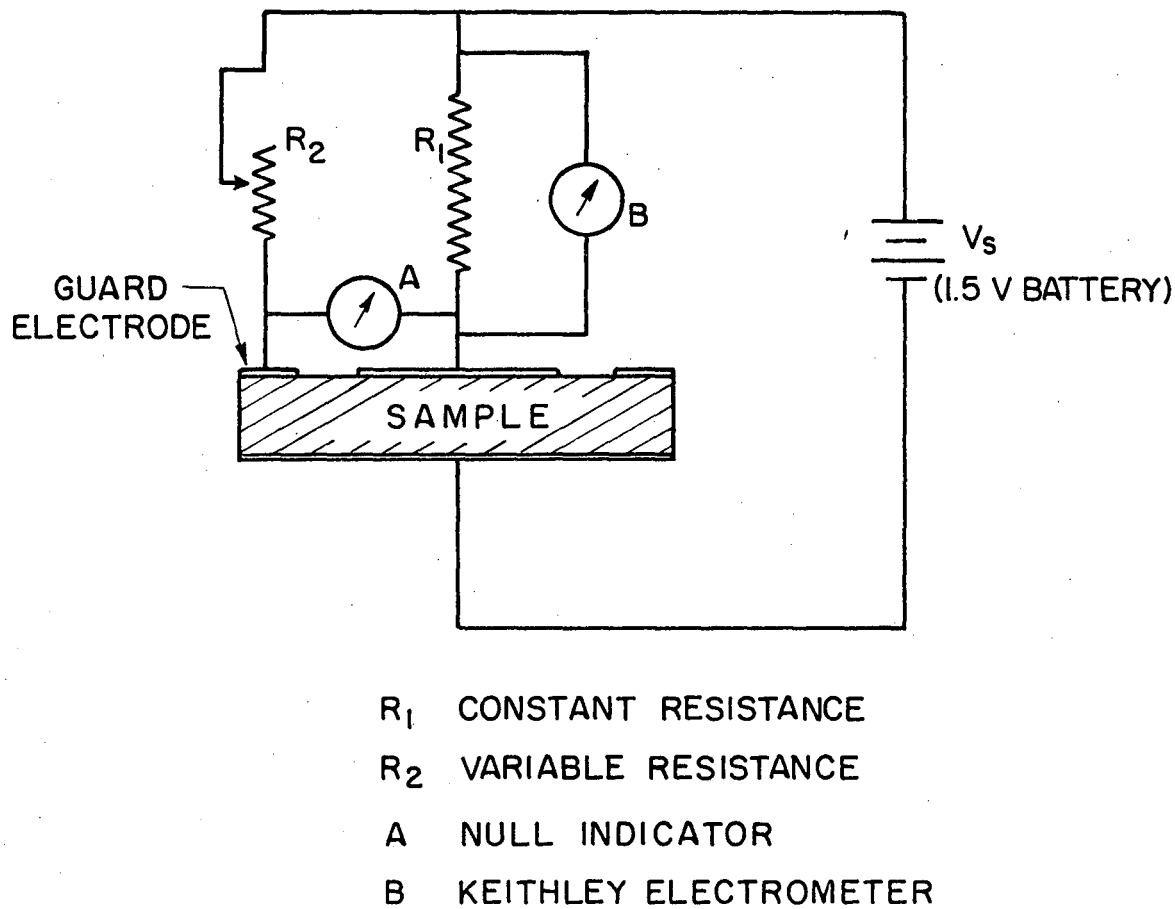

Fig. 12. Guard ring set up for dc resistivity measurement.

these measurements was 0.8 in. O.D., 0.5 in. I.D. and 1/4 in. thick. Sixty turns of copper magnet wire were used in both primary and secondary windings.

C. Results and Discussion

(1) Isothermal Sintering

Coble[17] has derived the following relation for bulk diffusion sintering applicable to later stages

$$d\rho/dt = ND\gamma\Omega/l^3kT \qquad (8)$$

where $d\rho/dt$ is the densification rate, N is a numerical constant, D is the diffusion coefficient, γ is the surface energy, Ω is a vacancy volume, l is the grain size and kT has the usual significance. If we assume that at a particular density, where discontinuous grain growth has not started, the average grain size is always the same irrespective of the temperature at which the sintering has been carried out, Eq. (8) can be integrated. Then on rearrangement and substituting $D = D_o \exp(-Q/kT)$ one can get

$$T/t = (N\gamma\Omega D_o/(\rho-C)kl^3)\cdot\exp(-Q/kT) \qquad (9)$$

where C is an integration constant. Thus we should be able to determine the activation energy for the rate controlling diffusional process from the slope of log(T/t) vs 1/T plot. This plot is shown in Fig. 13 for a density of 95% of the theoretical value and the actual data are summarized in Table IV. The activation energy is found to be 143±15 kcal/mol.

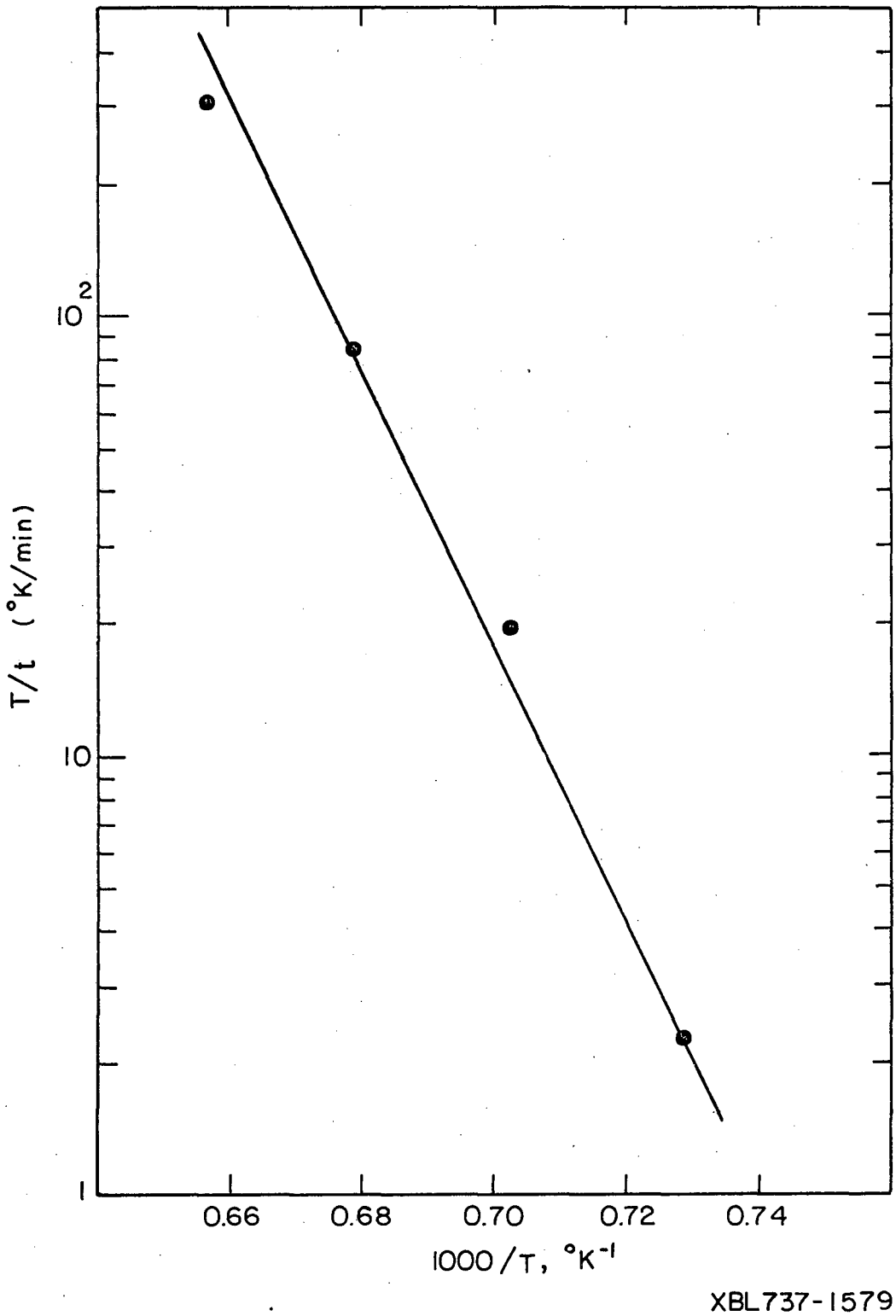

Fig. 13. Log (T/t) vs 1/T relationship for specimens with 95% theoretical density. Sintering runs were done in 1 atm oxygen and with stoichiometric packing powder. Activation energy for the sintering, determined from the slope, is 143 kcal/mol.

Table IV. Time-temperature data to attain 95% of theoretical density in some isothermal sintering runs

Temperature °K (T)	$10^3/T$ °K^{-1}	Time in minutes to attain 95% TD (t)	T/t °K/min
1373	0.7283	610	2.255
1423	0.7027	72	1.979 x 10
1473	0.6789	18	8.190 x 10
1523	0.6566	5	3.046×10^2

The assumption of constant grain size, which has been made above, was found to be reasonable. The microstructural studies revealed an average grain size of 3-5 microns in all the specimens at 95% TD.

(2) Nonstoichiometry and Its Relation to Densification and Microstructure

The effect of nonstoichiometry on the sintered density and microstructure of ferrites was first reported by Stuijts.[18,19] Reinjnen[20-22] afterwards presented an adequate theoretical model along with the experimental support, based on the assumption of volume diffusion, to describe the influence of stoichiometry on the sintering of spinels, oxides and oxidic compounds. Readey[23] also calculated the dependence of volume diffusion on small deviations from stoichiometry. In Reinjnen's analysis it was assumed that, in the spinels diffusivity of oxygen, (D_{oxygen}) is much smaller than the diffusivity of cations (D_c). Under this condition, it was shown that the anion vacancy flux reduces drastically in the region of excess cation vacancies. He showed, in the case of $NiAl_2O_4$, a drastic drop in the sintered density occurred in the excess Al_2O_3 compositions which is the cation deficient side of the system. But the density drop was much less drastic in the $NiFe_2O_4$ system under the same conditions. This was explained on the basis that Fe_2O_3 is mainly dissolved as Fe_3O_4 and partly as Fe_2O_3. Sintering at high temperatures results in further reduction of Fe^{+3} to Fe^{+2} by the reaction

$$Fe^{+3} + 3/8V_c + 1/2\ O^{-2} \rightleftarrows Fe^{+2} + 1/4\ O_2(g) \qquad (2)$$

and thus a large part of the excess cation vacancies are annihilated

resulting in an increase of anion vacancy concentration. Stuijts[24] later on reviewed Reinjnen's results and showed strikingly similar behavior in the densification of a Ni-Zn ferrite composition with the theoretical plot of Reinjnen.

Similar studies on the lithium ferrite system have been done in this investigation. Figure 14 shows the relationship between the sintered density and the composition of the green compact (solid line). As is expected, maximum density was obtained slightly on the lithia rich side. It is also clear that the density drops significantly in the Fe_2O_3 excess region.

The microstructural characteristics observed in these sintered specimens are also in agreement with Stuijts'[18,19] and Reinjnen's[20] observation for other ferrites. As shown in Fig. 15, compositions with excess Fe_2O_3 showed a microstructure with large pores exclusively at the grain corners. On the other hand, the lithia rich compositions showed discontinuous grain growth with pores entrapped within the grains.

This behavior has been explained by Reinjnen[20] through a model where oxygen can be transported over the gas phase, whereas cations diffuse through the bulk. It has been shown[20] that in cation deficient compositions, pores can move with the grain boundary more easily and thus exaggerated pore growth may occur. On the other hand, in anion deficient compositions, discontinuous grain growth is favored.

In all the above runs, stoichiometric packing powder and 1 atm O_2 were used for atmosphere control. For the varying composition packing powders, stoichiometric specimens were used. In Fig. 14, density values have been plotted against the composition of the packing powder (dashed

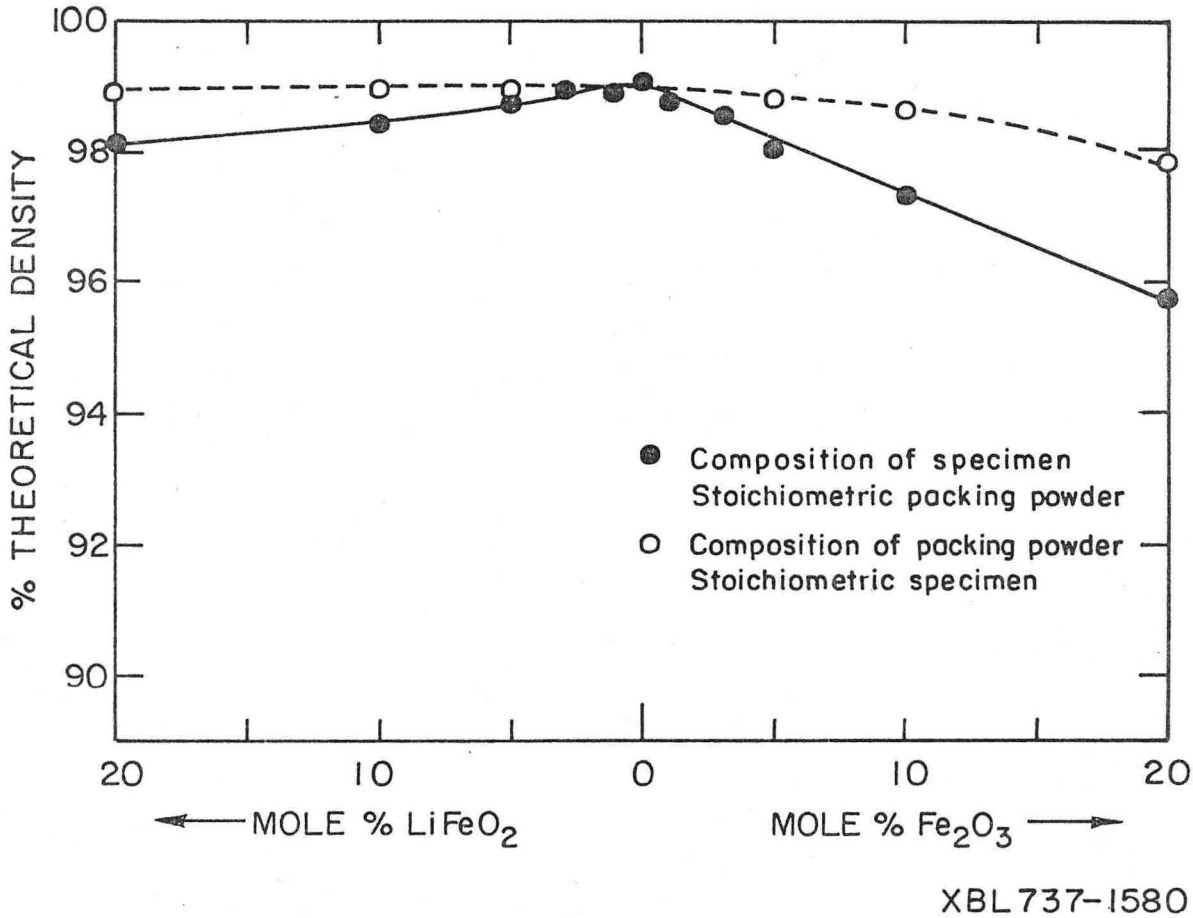

Fig. 14. Variation of the sinter density with the composition of the specimen, and also with the composition of the packing powder. Sintering conditions were 1150°C for 2 h in 1 atm oxygen.

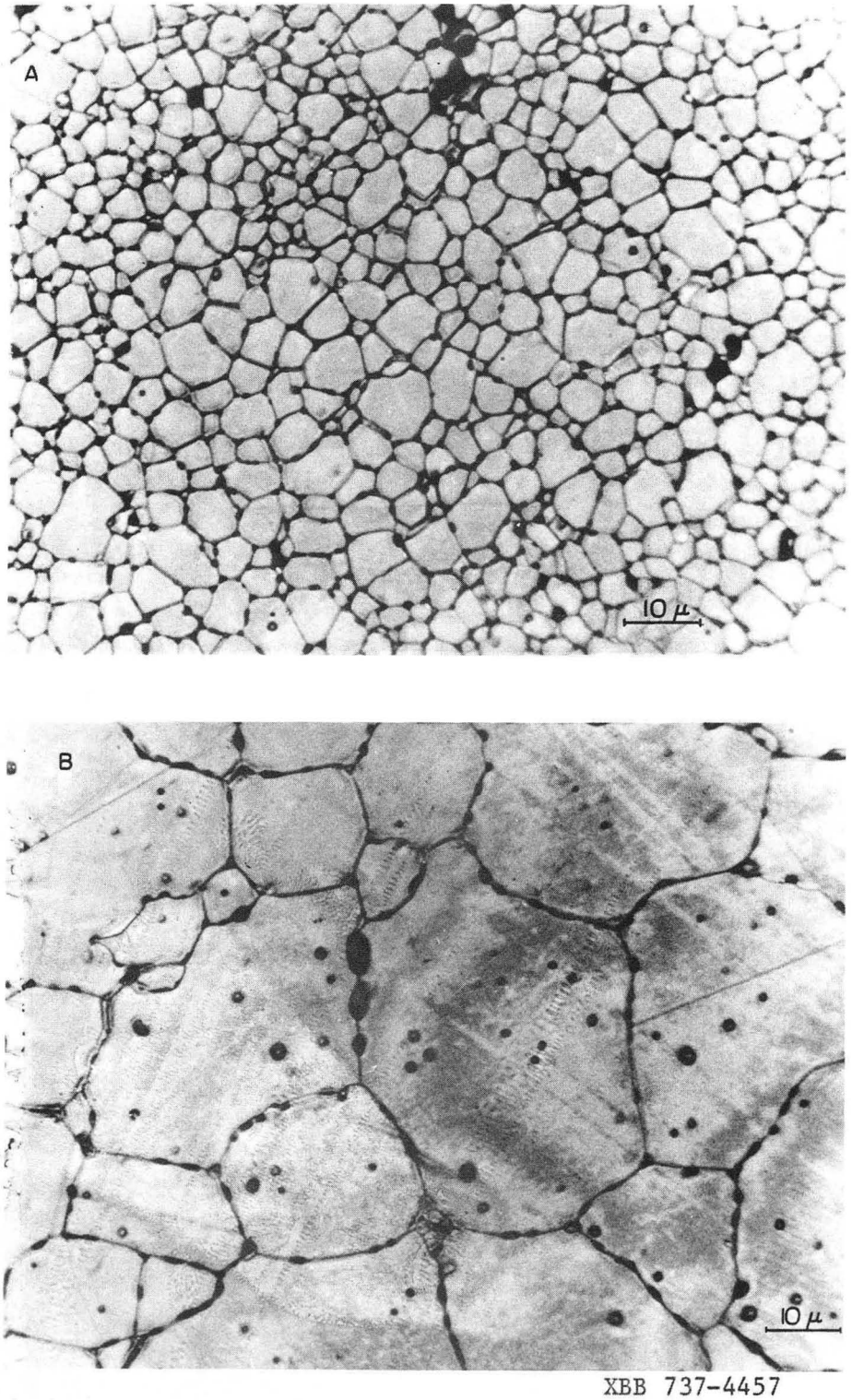

XBB 737-4457

Fig. 15. Dependence of the microstructure on the stoichiometry. (A) $LiFe_5O_8$ + 1 mol% Fe_2O_3, (B) $LiFe_5O_8$ + 1 mol% $LiFeO_2$. Sintering runs were done at 1150°C for 2 h in 1 atm O_2 and using stoichiometric packing powder.

line). It is expected that with a Fe_2O_3 rich packing powder some lithia will be lost from the specimen, thus leading to an excess Fe_2O_3 in the specimen composition. On the other hand, the lithia content may be kept constant in the specimen with the lithia rich packing powder. Since the excess Fe_2O_3 in the former composition would mean a higher cation vacancy concentration (and hence a lower anion vacancy concentration), a lower density is expected when Fe_2O_3 rich packing powders are used in the sintering runs. The insignificant density difference as observed at 1150°C (Fig. 14) may be due to the loss of excess cation vacancies through the oxygen loss by reaction 2. Thus if the oxygen loss could be avoided by using a lower sintering temperature so that the cation vacancies would remain low, a significant density difference should be observed depending on the packing powder composition. This has been found to be true, as shown in Fig. 16 where Lacy's[25] data has been plotted. It is clear that sintering at 1000°C results in a density difference of about 10%, whereas at 1100°C almost the same densities are attained under both conditions.

(3) X-ray Results

The phase equilibria in the system Li_2O-FeO-Fe_2O_3 has been studied by various workers.[15,26,27] But still the details of the phase diagram and also most of the thermodynamic data on this system are not available in the literature. X-ray diffraction is very commonly used to identify various phases. But in this particular system, it is quite difficult to distinguish one phase from another by X-ray diffraction, because the important X-ray peaks for most of the possible phases (e.g.

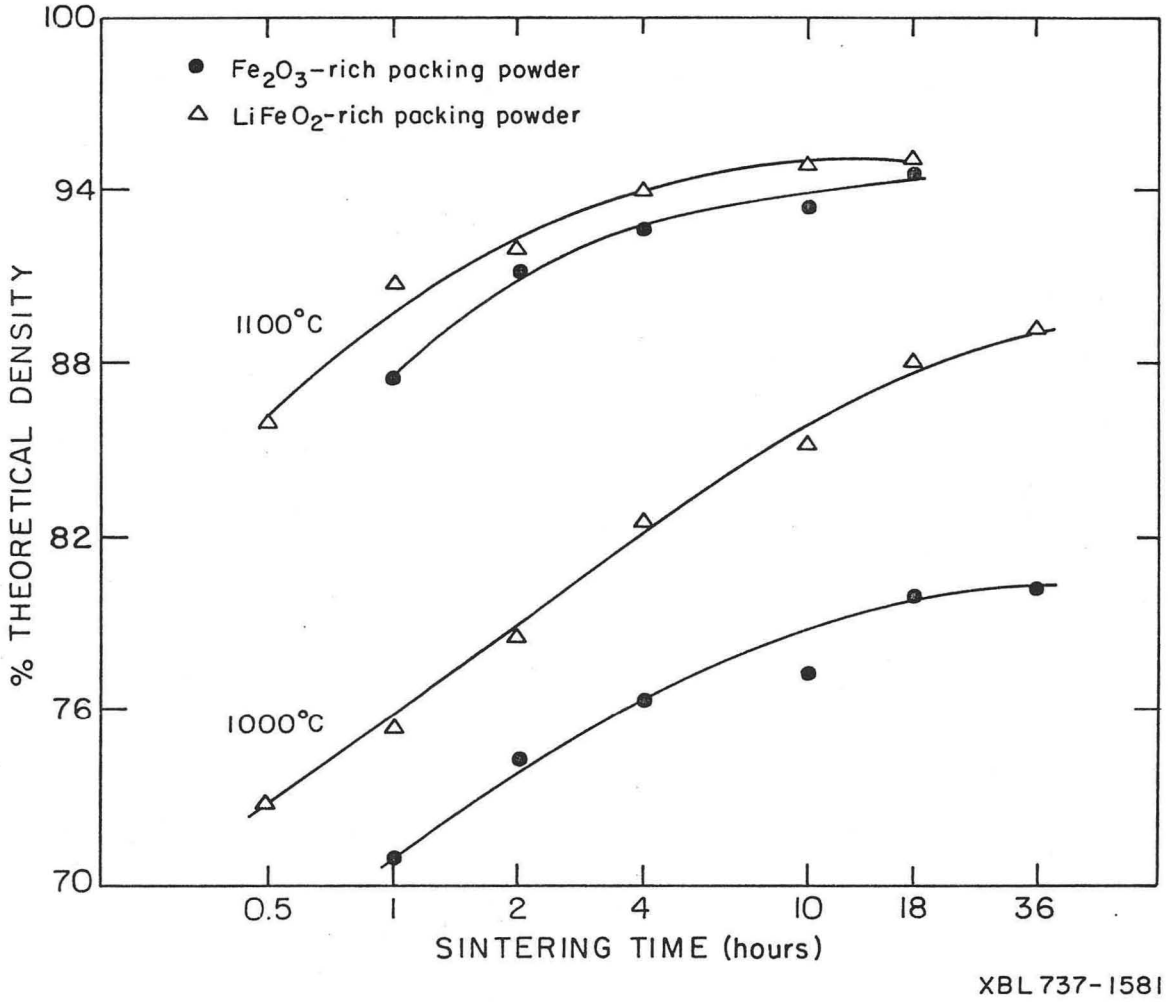

Fig. 16. Density-time relationship for some isothermal sintering runs of stoichiometric specimens in two different packing powder atmospheres and at 1 atm oxygen.[25]

$LiFe_5O_8$, $LiFeO_2$, Fe_3O_4, etc.) overlap on one another. But by the use of I_{311}/I_{400} (both the planes are for the spinel phases Fe_3O_4 and $LiFe_5O_8$; the (200) peak of $LiFeO_2$ overlaps with the (400) peak of the spinel phases), qualitative information about the relative amounts of spinel phase and $LiFeO_2$ phase can be obtained by measuring integrated intensities. A high value of the ratio indicates the predominance of the spinel phases whereas a low value would mean a large amount of $LiFeO_2$ in the composition. In Fig. 17, I_{311}/I_{400} ratio for the surface of the sintered ferrites has been plotted against the composition of the green compact. Predominantly spinel phase was observed on the Fe_2O_3 rich side of the composition and $LiFeO_2$ phase on the lithia rich side. The interior of all these specimens was X-rayed after grinding off the surface. In each case it showed X-ray peaks typical of the spinel phase. The composition variation at the surface of the sintered specimens is obviously due to the material loss from the system. Salmon and Marcus[28] first postulated the following reactions while studying the lithium loss behavior from a Li-Ni ferrite composition.

$$6LiFe_5O_8(s) \rightleftarrows 6LiFeO_2(s) + 8Fe_3O_4(s) + 2O_2(g) \qquad (10)$$

$$6LiFeO_2(s) \rightleftarrows 2Fe_3O_4(s) + 3Li_2O(g) + 1/2\ O_2(g) \qquad (11)$$

Thus, according to these reactions, with the initial oxygen loss from the stoichiometric composition, $LiFeO_2$ phase should start to appear. If the conditions are such that the lithia loss is not possible by

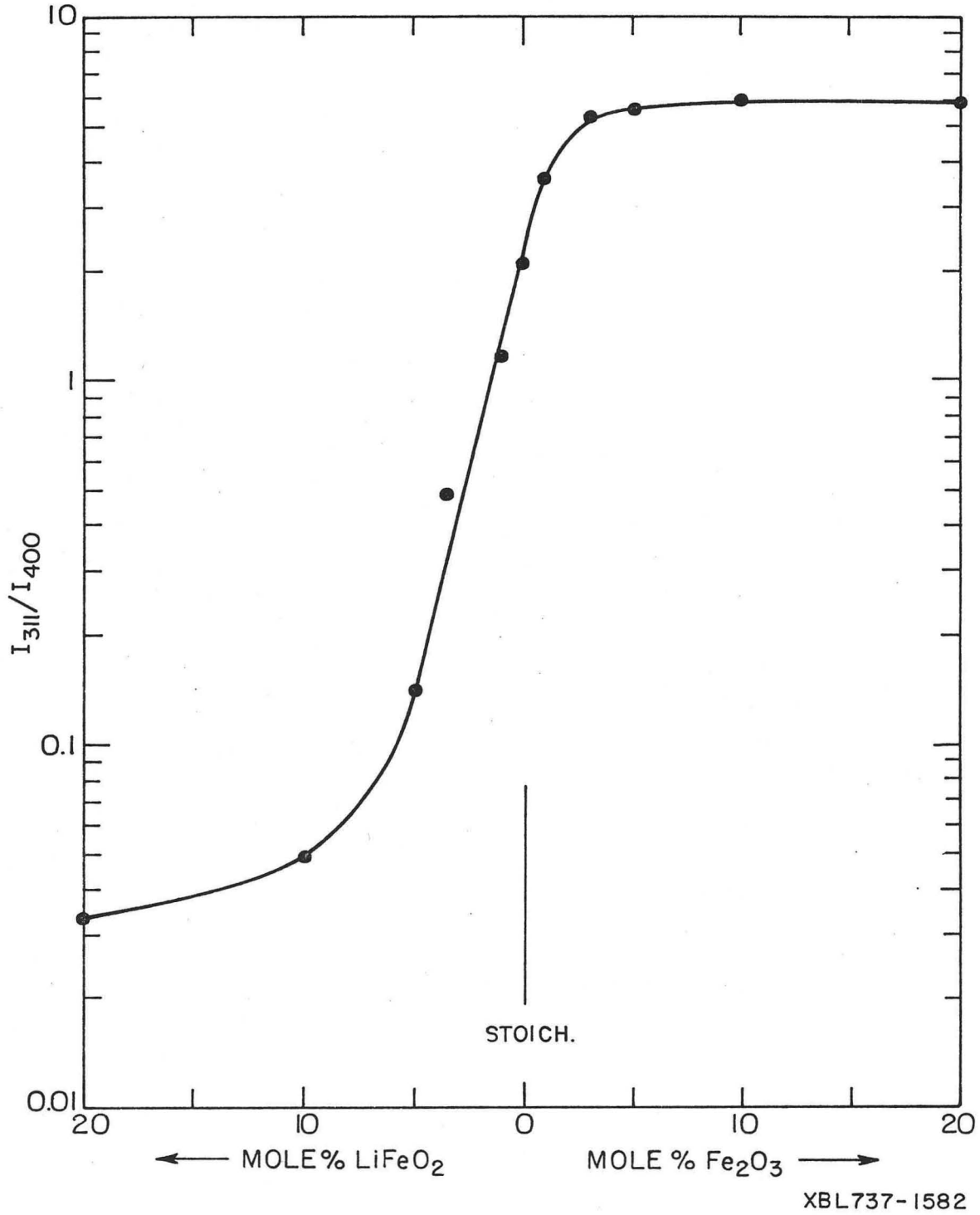

Fig. 17. X-ray data for specimens sintered at 1150°C for 2 h in 1 atm oxygen using stoichiometrick packing powder.

reaction 11, Fe_3O_4 may react with lithia and oxygen from the surrounding atmosphere forming $LiFeO_2$ following reaction 11 in the reverse direction. Part of Fe_3O_4 may go in solid solution with $LiFeO_2$ as FeO. Thus a surface composition with no or very little spinel phase may be obtained. Apparently this is what happens with lithia excess composition. For Fe_2O_3 excess compositions, it appears as if Fe_2O_3 goes into solid solution with spinel $LiFe_5O_8$ as Fe_3O_4, and then the process stops unless the sintering temperature is high enough or the time at temperature is long enough to support further oxygen loss or lithia loss from the system. In Fig. 18, I_{311}/I_{400} ratio has again been plotted against sintering time at various temperatures. The green specimens in these runs were stoichiometric. The initial drop of the intensity ratio is probably due to the start of the reaction 10 where $LiFeO_2$ is formed. At higher temperature sintering runs (e.g. at 1150°, 1250°C), the ratio starts to increase again indicating the increase in the spinel content of the composition. This is probably because the lithia loss through reaction 11 gradually becomes significant at this point.

Predominantly spinel phase in the bulk composition is attributed to the very little material loss from the bulk region due to the formation of protective reacted layers.

(4) DC Resistivity

The reason that the spinel ferrites are important in many magnetic applications is the fact that the electrical conductivity of the ferrites is considerably lower than that of the magnetic metals. Thus these have the advantage of significantly lower power loss. Resistivity of these systems acts as one of the most important characterizing parameters.

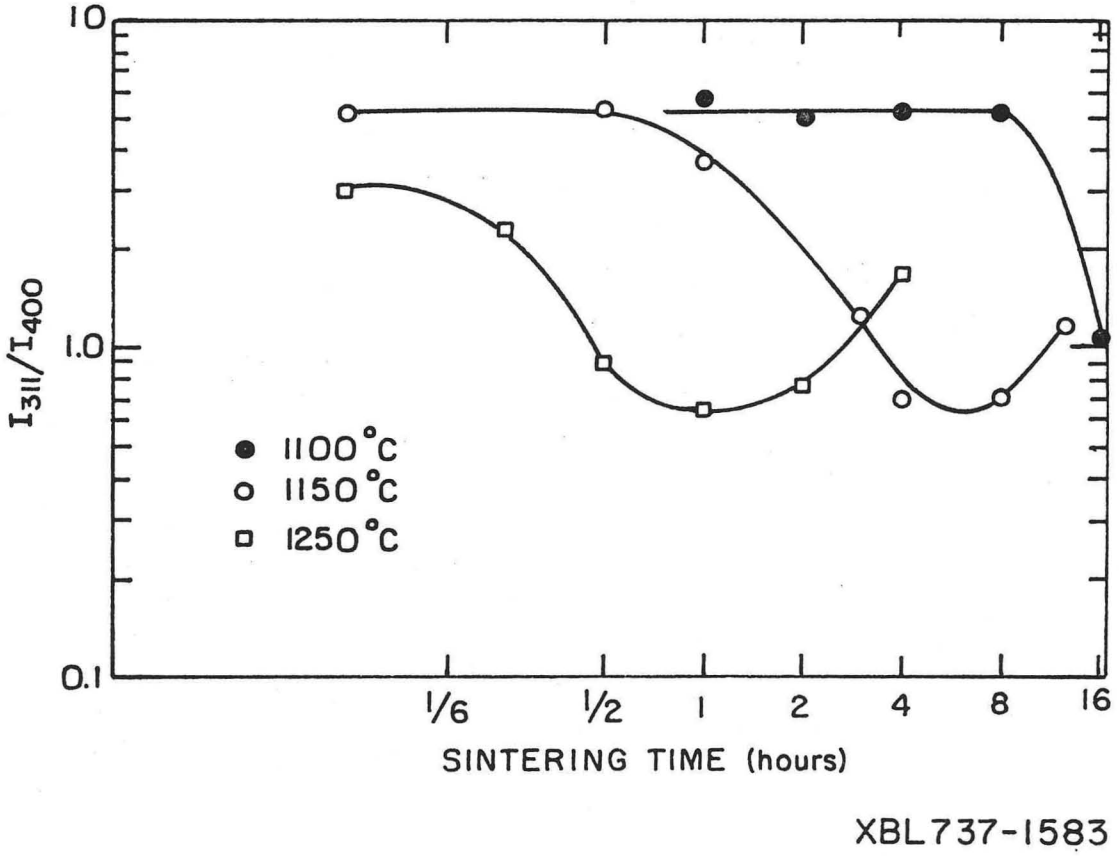

Fig. 18. X-ray data for isothermally sintered specimens. Sintering runs were done in 1 atm oxygen and with stoichiometric packing powder.

"Ferrites" in general can be classed as "low mobility materials." In recent years, considerable interest[29-33] has been shown in this type of compound and it has been indicated that the standard band theory argument may not be applicable for these materials. The theory to explain this was first presented by Mott.[34] The basic idea was, for less than a critical band width, the material will become insulating even with the existence of a partially filled band. The most common examples of this class are in the transition metal oxides. It is believed that in these materials, overlap of the partially filled d orbitals is small due to the relatively large separation between the transition metal cations amongst which the charge transfer occurs. Presence of oxygen ions perturbs the system further. These factors lead to very narrow bands. So the decrease in energy due to the band formation may be quite small compared to the increase of the correlation energy which arises due to the possibility of two electrons correlating their motion to avoid each other spatially and thereby reducing their mutual coulomb repulsion. Most band calculations are based on one electron approximations and thus neglect this correlation energy term. This assumption is valid as long as wide band materials are considered. But this correlation energy cannot be ignored for the case of transition metal oxides or rare earth compounds. This it is clear that in these compounds electrons tend to localize in a region and for a transport process to occur an activation energy barrier must be overcome so that the electron can hop to another favorable site.

In an ionic solid a further possibility is the formation of "polaron" which is defined[35] as the combination of the electron with its

strain field. In a narrow band solid "small polarons" may form which would be trapped in the vicinity of a particular lattice site and would require a certain activation energy, as mentioned above, for acting as carriers. This type of conductivity process, where localized carriers are involved, is commonly known as the "hopping conductivity mechanism." (Localization of electrons through polaron formation or through disorder has been extensively discussed in the literature. See, for example, the article by Austin and Mott.[36])

The semiconduction properties of lithium ferrite have received some attention in the literature.[7,36-39] It has been established[37-39] that electrons hopping from Fe^{+2} to Fe^{+3} act as the primary charge transfer process. Wang et al.[37,38] in their investigation described oxygen vacancies as the minor carriers. But the primary problem in explaining the conduction behavior in lithium ferrite is due to the lack of understanding of the origin of hopping energy. In this investigation, no attempt has been made to solve this problem. But data have been presented to show the influence of stoichiometry (which directly affect the carrier concentration) on the dc resistivity value of polycrystalline ferrites and the results have been analyzed on the basis of the above mechanisms. Also, the data related to the influence of the sintering conditions and the microstructure on the observed resistivity value have been discussed.

The influence of composition on the dc resistivity value of sintered polycrystalline lithium ferrite has been shown in Fig. 19. Both the bulk and the surface resistivity values are plotted. The sharp drop in the resistivity value while moving into the cation deficient region

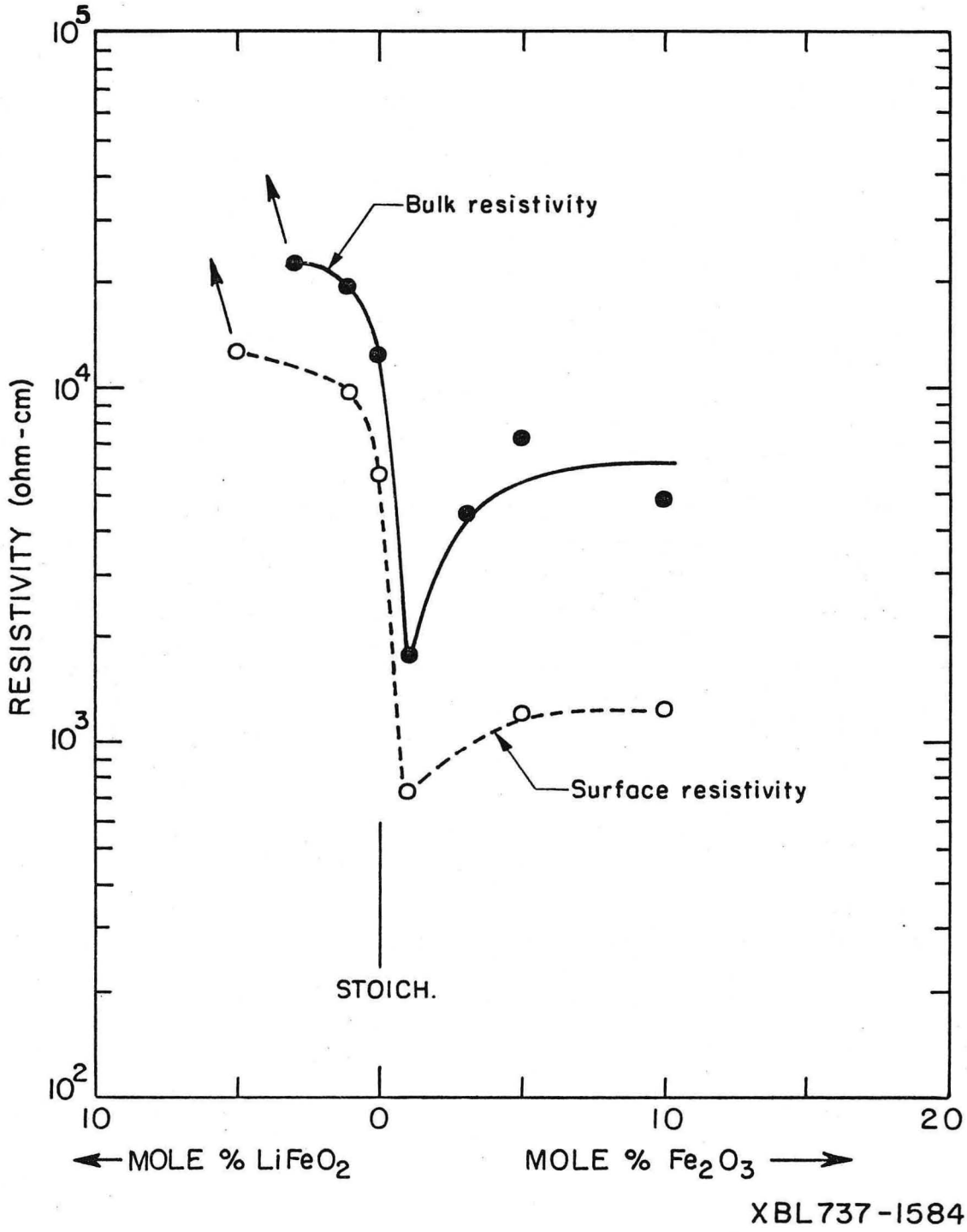

Fig. 19. Dependence of bulk and surface resistivity on the stoichiometry of the specimen. Sintering conditions were: temperature = 1150°C, time = 2 h, atmosphere = 1 atm oxygen and stoichiometric packing powder.

is similar to that observed for Ni-Zn ferrite[40] or for cobalt ferrite.[41] In Ni-Zn ferrite or cobalt ferrite, it has been shown that hole conduction due to Ni^{+3} or Co^{+3} dominates on the anion deficient side and electron conduction (due to Fe^{+2}) dominates in the cation deficient region. The situation is somewhat different in the case of lithium ferrite where, unlike nickel or cobalt, lithium is monovalent and does not change valency. Another important point of difference is the tendency of order[1] in the octahedral region, which also has a strong influence on the conductivity value.[7,38,42] In any event, as has been mentioned earlier, electron hopping from Fe^{+2} to Fe^{+3} is assumed to be the primary charge transfer mechanism in the conduction process of lithium ferrite. For dc conductivity and for one type of charge carrier

$$\sigma = ne\mu \tag{12}$$

where n is the number of carriers and can be related to the number of Fe^{+2} ions in the octahedral site, e is the electronic charge and μ is the mobility of the electrons in the system. Jonker[41] expressed carrier mobility in cobalt ferrite by a diffusion type expression

$$\mu = (ed^2\nu/kT)\cdot\exp(-q/kT) \tag{13}$$

where d is the jump length, ν is the lattice frequency active in the jumping process and q is the activation energy for the jump. With increasing Fe_2O_3 in the composition, more and more Fe^{+2} would be active in charge transport. But at the same time Fe^{+2} in the octahedral region

would tend to introduce some disorder in the system. As suggested by Austin and Mott[36] this disorder may contribute to the activation energy term (q) in the mobility expression (Eq. (13)), and thus decrease the mobility of the carrier. The sharp drop in resistivity in the cation deficient region as shown in Fig. 19 is probably due to the increase in the number of charge carriers. But the changes that are observed away from the stoichiometric line can be due to a combined effect of mobility and charge carriers. In the anion deficient side, oxygen vacancies may act as the major carriers. But it is accepted[15] that too great a deviation from stoichiometry in the oxygen deficient region is unfavorable in lithium ferrite. Thus second phases show up rather quickly as has been confirmed by the microstructural investigation, and the resistivity of the system tends to increase.

Until now we have considered the resistivity problem only from the standpoint of carrier concentration and mobility. For a polycrystalline sintered specimen, the problem may increase manyfold. In Fig. 20 average size of the largest grains and dc resistivity have been plotted against sintering time in isothermal sintering runs. It is clear that discontinuous grain growth is always accompanied by an increase of resistivity value. This is possible only if grain boundaries act as the easy conducting path compared to the bulk of the grains. This may be due to higher carrier concentration at the boundaries because of preferential material loss from or along the grain boundaries. The subsequent decrease in resistivity with increasing sintering time can be related to the increased density or to the increased carrier concentration due to continued material loss.

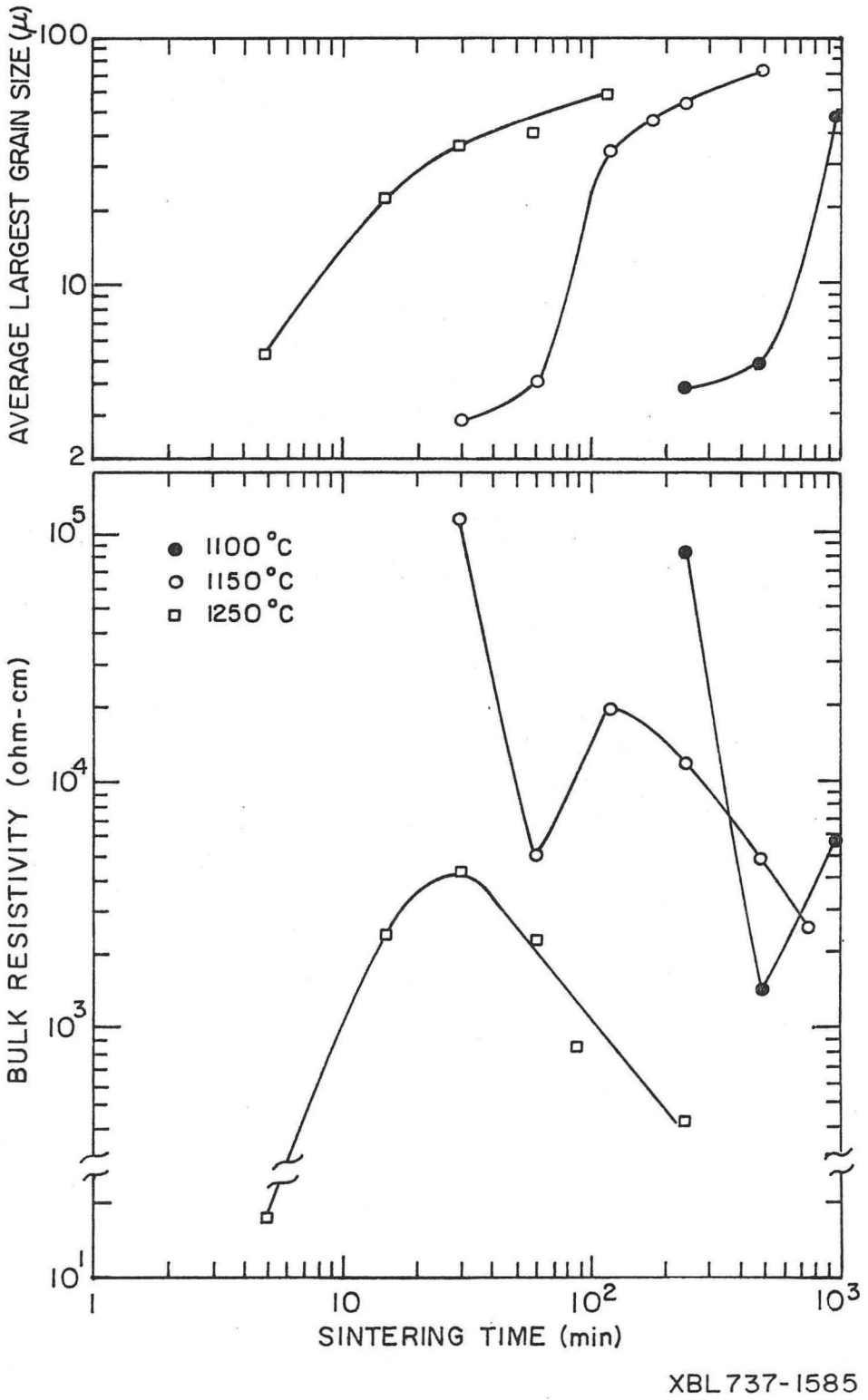

Fig. 20. Grain size and bulk resistivity data from some isothermal sintering runs. Stoichiometric packing powder and 1 atm oxygen were used in all the sintering runs.

(5) B-H Loop Parameters

It has been reported in the literature[3-8] that with proper processing and with selected dopants, very good square loop materials can be obtained from lithium ferrite compositions. The use of the packing powder method for the processing of lithium ferrite also gave very good square loops. In most of the cases, the squareness R_s, which has been defined as the ratio of the remanent induction to the maximum induction (B_{max}), was found to be better than 0.85.

The influence of composition on the coercive force (H_c) is shown in Fig. 21 (solid line). Decrease of H_c on the anion deficient region is probably due to the increased grain size. Compositional effect on the squareness or B_{max} value was found to be insignificant. The influence of the packing powder composition on the H_c value of the specimens sintered from the stoichiometric green compacts has also been shown in Fig. 21 (dotted line). Lower values of H_c were obtained by the use of lithia rich packing powder. One specimen was sintered in 1 atm O_2 without any packing powder. H_c value for this specimen has been represented by the star (*) in Fig. 21.

The effect of sintering time and temperature on the hysteresis loop parameters is shown in Fig. 22. H_c drops to a low value with increasing time and temperature, B_{max} reaches a more or less constant value after long time sintering at any temperature. But squareness (R_s) showed a maxima with sintering time. These variations are probably a combined effect of density and microstructure evolution. With increasing density all the hysteresis loop parameters improve. But the strongest influence of the microstructural characteristics is probably on the H_c

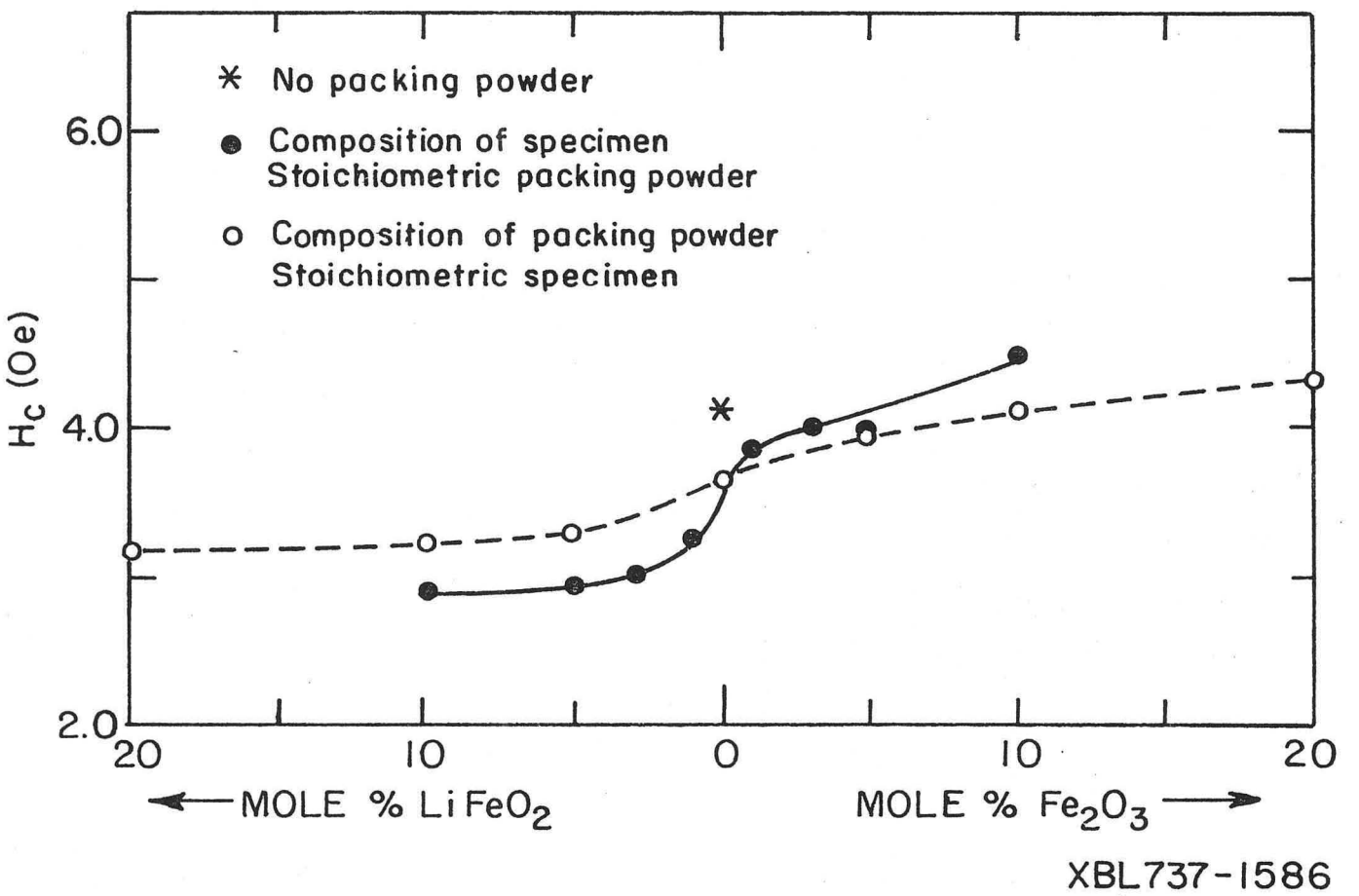

Fig. 21. Variation of coercive force (H_c) with the composition of the specimen, and also with the composition of the packing powder. Specimens were sintered at 1150°C for 2 h in 1 atm oxygen.

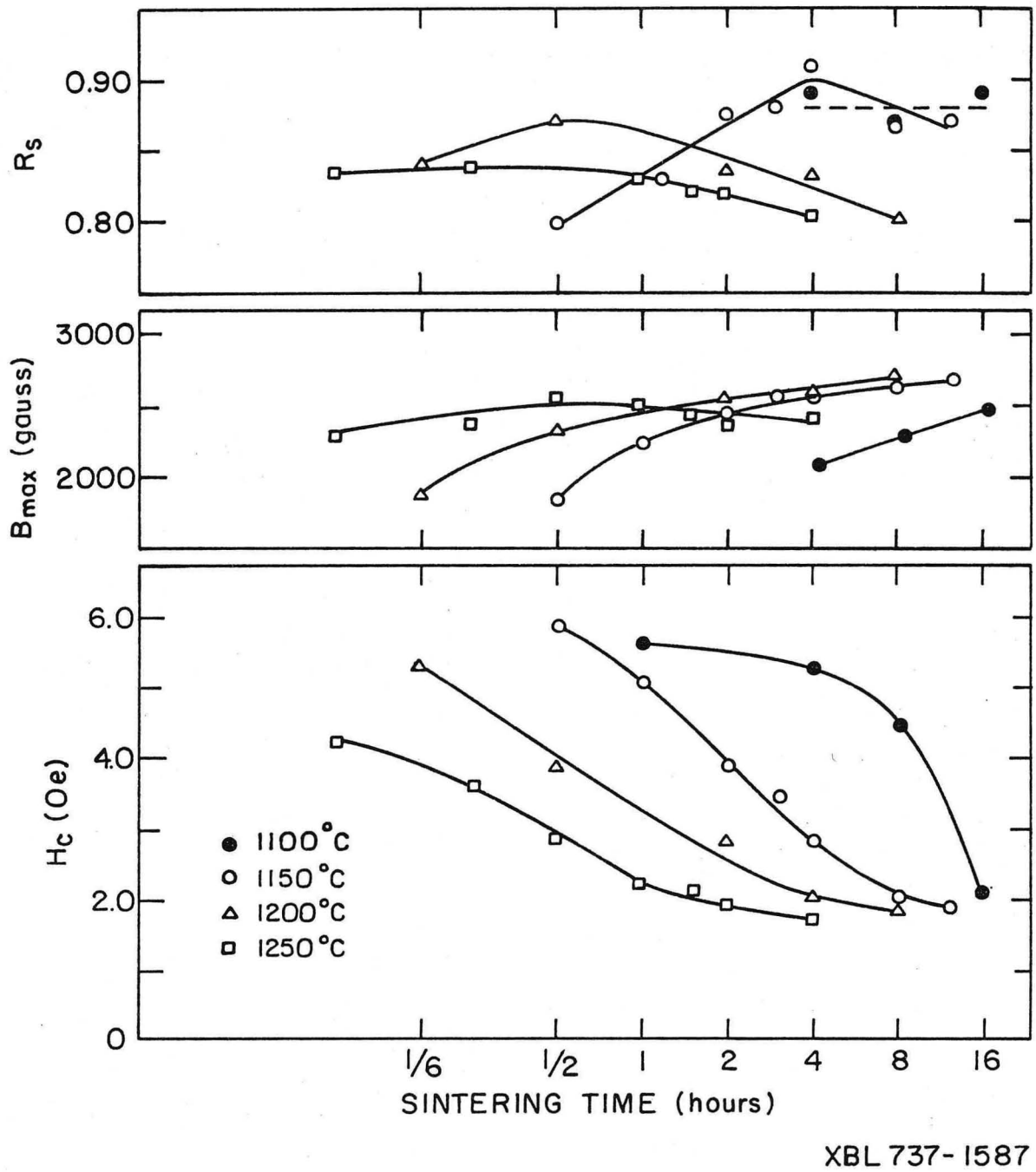

Fig. 22. Variation of B-H loop parameters with sintering time in some isothermal sintering runs. Stoichiometric packing powder and 1 atm oxygen were used in all these runs.

value, and thus in most of the above cases we see a drastic variation of the coercive force with the processing parameters.

IV. EFFECT OF DOPANTS

A. Introduction

In the preceding sections it has been established that significant material loss can occur during the sintering of lithium ferrite. By proper control of sintering parameters and stoichiometry, the properties of the final sintered ceramic can be controlled to some degree. Working with the intrinsic material places a limit on the stoichiometry control that can be achieved. Thus in the processing of ceramic materials, it is very often desirable to add small amounts of selected additions to control the sintering, microstructure developed and the physical and chemical properties. Dopants may modify the sintering behavior and the microstructure, which in turn, may influence the properties of the final ceramic. On the other hand, some dopants may directly influence the properties through other parameters without influencing the densification or microstructure. In the case of lithium ferrite, it has been demonstrated that small additions of nickel,[3] zinc,[7] nickel and zinc,[5] and manganese[6,8] significantly improve the hysteresis loop squareness. However, none of these studies investigated the influence of the dopants on the densification and microstructure. In a recent study[43] carried out in this laboratory, it was noted that, depending on the atmosphere of sintering, dopants like NiO, MgO or TiO_2 can enhance the grain growth rate in lithium ferrite. It was further noted that the extrinsic defects introduced by these dopants may not have a significant effect on the densification compared to that due to the intrinsic defects in the composition. Thus it was felt necessary that to explain the effect of the dopants on the electrical and magnetic properties (i.e. dc resistivity

or hysteresis loop parameters) of ferrites, one should also take into consideration the influence on the densification and microstructure. In this section, a systematic study of the influence of varying amounts of NiO and $NiFe_2O_4$ dopants on the densification, microstructure, dc resistivity and B-H loop parameters has been made. Thermogravimetry and X-ray diffraction were used to characterize the chemical changes during processing.

B. Experimental Procedure

The preparation of the lithium ferrite powder was identical to that described in the earlier sections. $NiFe_2O_4$ powder was prepared by using reagent grade NiO and Fe_2O_3 as the starting material. Mixing was done in a neoprene lined ball mill for 48 h using isopropyl alcohol and teflon balls. The alcohol was evaporated and the mixture was calcined at 950C for 5 h in air. The calcined powder was milled and was recalcined at 1000C for 4 h in 1 atm O_2.

A controlled amount of NiO or $NiFe_2O_4$ was added to the lithium ferrite powder and the mixture was mixed for 24 h in isopropyl alcohol. For the thermogravimetric runs, a second calcination of the powder mixture was carried out at 800C for 6 h in 1 atm O_2.

Specimen size and its preparation for the sintering runs are the same as described earlier. Most of the sintering runs were made at 1150C for 2 h in 1 atm O_2 using a stoichiometric packing powder.

The techniques for the property measurements, the weight loss apparatus, and the experimental conditions associated with the thermogravimetric runs are also described in the earlier sections.

C. Results and Discussion

(1) Densification and Microstructure

In Fig. 23 the sintered densities of the doped specimens have been plotted against the amount of dopants after sintering at 1150°C for 2 h. For both NiO and $NiFe_2O_4$, a drop in density is observed. In the case of NiO, this drop in density is probably due to the beginning of discontinuous grain growth with increasing amounts of NiO (Fig. 24). Discontinuous grain growth would cause a larger amount of pores to be entrapped within the grains, thus leading to a lower final density.

The occurrence of discontinuous grain growth with increasing NiO content can be accounted for by the hypothesis that NiO reacts with $LiFe_5O_8$ following the reaction,

$$2NiO + LiFe_5O_8 = 2NiFe_2O_4 + LiFeO_2 \qquad (14)$$

thereby forming $LiFeO_2$ in the specimen. In cases where NiO remains in solid solution with lithium ferrite, oxygen vacancies should be formed with excess cations in the interstitials. In either of the above cases where either oxygen vacancies or $LiFeO_2$ or both are formed, enhanced grain growth would be favored. The proposed reaction (reaction 14) can be supported through the thermogravimetric analysis of NiO containing compositions. $LiFeO_2$, if formed, would alter the weight loss behavior of the powder significantly. In Fig. 25 weight loss data in mgs/mole of powder of 3 and 10 mol% NiO in lithium ferrite have been plotted against temperature, along with that for stoichiometric lithium ferrite in constant heating rate runs. The weight loss behavior was identical

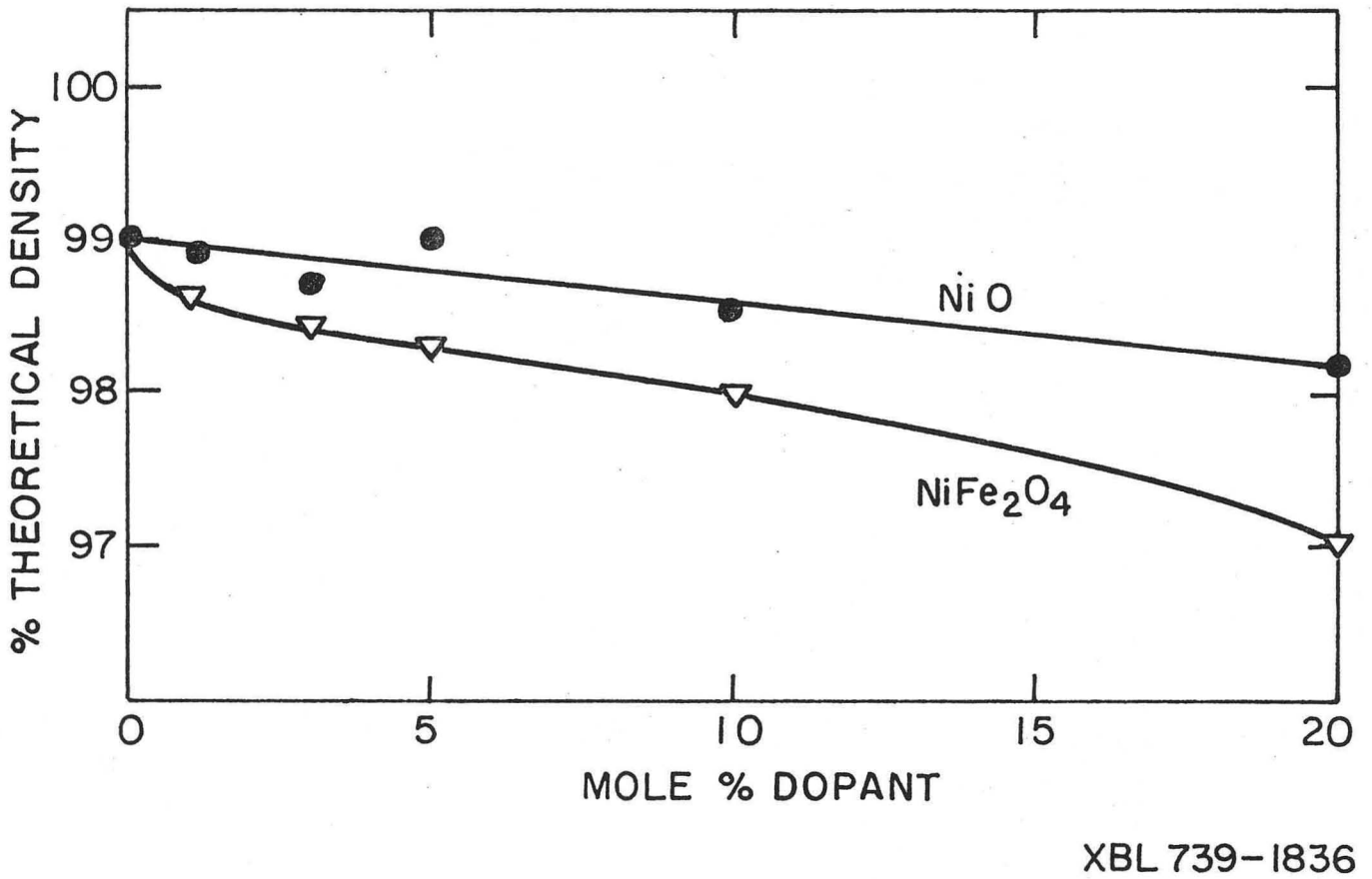

Fig. 23. Dependence of the sintered density on the amount of dopants. Sintering runs were done at 1150°C for 2 h in 1 atm O_2 and using stoichiometric packing powder.

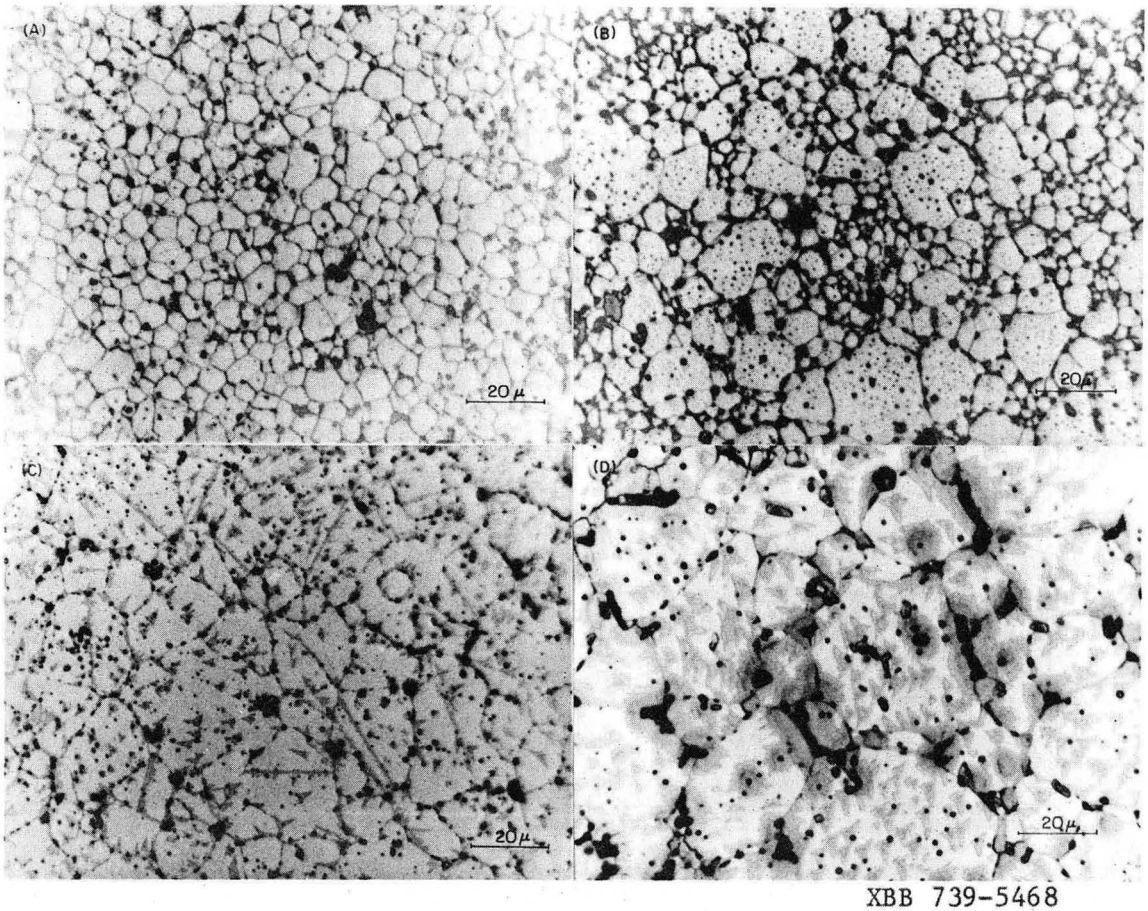

XBB 739-5468

Fig. 24. Influence of NiO dopant on the microstructure of the specimens sintered at 1150°C for 2 h in 1 atm O_2 and using stoichiometric packing powder. (A) 1 mol% NiO, (B) 3 mol% NiO, (C) 5 mol% NiO, (D) 10 mol% NiO.

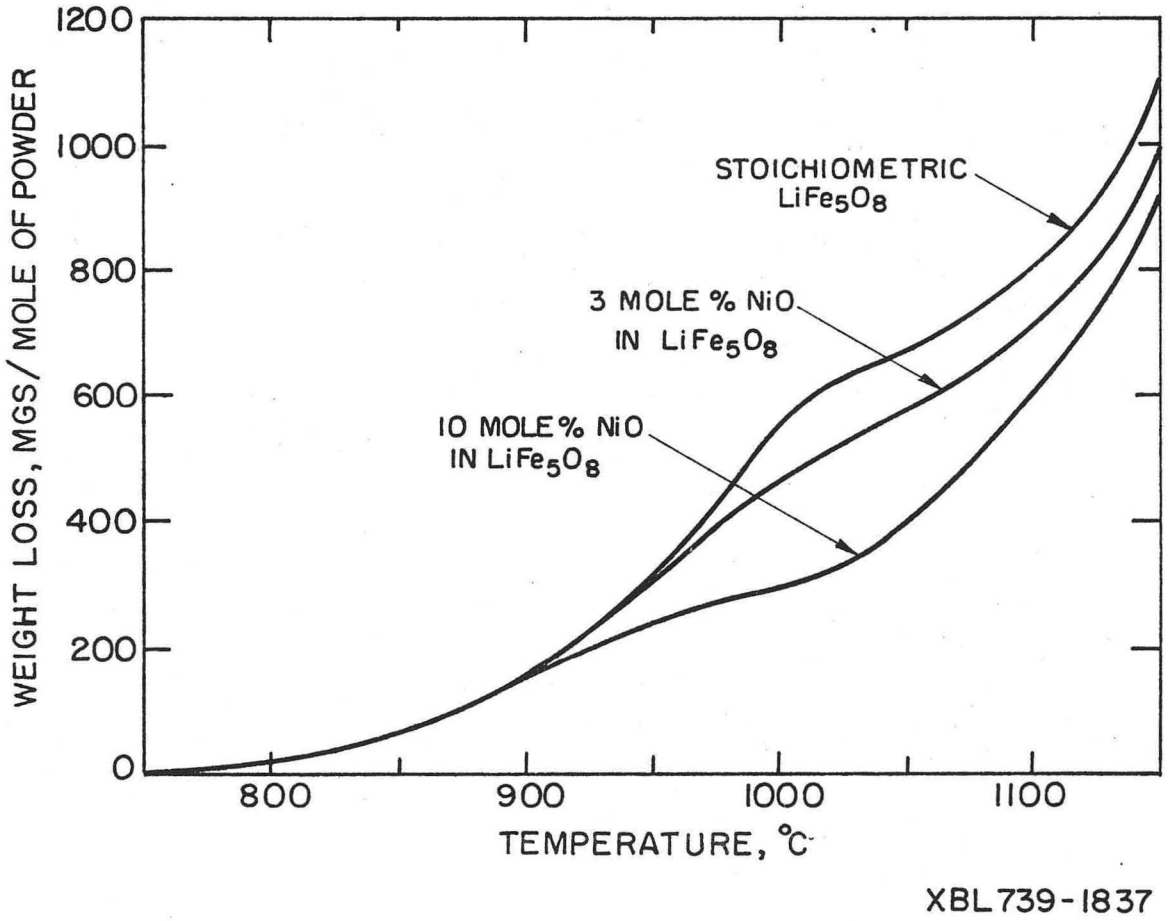

Fig. 25. Weight loss data in air for constant heating rate runs for lithium ferrite compositions with varying NiO content.

to those of excess $LiFeO_2$ (in $LiFe_5O_8$) compositions (see, for example, Fig. 2). The equilibrated weight loss values for 5 and 10 mol% NiO containing lithium ferrite have been plotted against 1/T in Fig. 26, along with those for 5 mol% $LiFeO_2$ in $LiFe_5O_8$ and 1 mol% Fe_2O_3 in $LiFe_5O_8$. It is interesting to note that NiO dopants in the composition retard the initial weight loss in the same way as is observed for excess $LiFeO_2$ (in $LiFe_5O_8$) compositions. The fact that 10 mol% NiO in $LiFe_5O_8$ and 5 mol% $LiFeO_2$ in $LiFe_5O_8$ compositions exhibit nearly identical weight loss behavior is in agreement with reaction 14, which suggests 2 moles of NiO react to form 1 mole of $LiFeO_2$.

Further support of reaction 14 can be obtained through the X-ray studies of the specimen surfaces sintered at 1150C for 2 h in 1 atm O_2 and using stoichiometric packing powder. In Fig. 27, the I_{311}/I_{400} ratio has been plotted against the dopant content in the composition. Decreasing spinel content (as is evident from the decreasing I_{311}/I_{400} ratio) on the surface with increasing NiO dopant in the composition is identical to that observed for specimens with excess $LiFeO_2$ in the composition (Fig. 17). It has already been shown that under the above experimental conditions, excess $LiFeO_2$ in the sample composition leads to a surface phase with very little spinel.

A "self decoration effect," as was observed by Lessoff and Childress[44] on the thermally etched surfaces of polycrystalline lithium ferrite, is also evident on the micrographs of 5 and 10 mol% NiO containing compositions (Fig. 24). A similar effect was also observed in lithia rich compositions (Fig. 28), but was never noted in cation deficient materials.

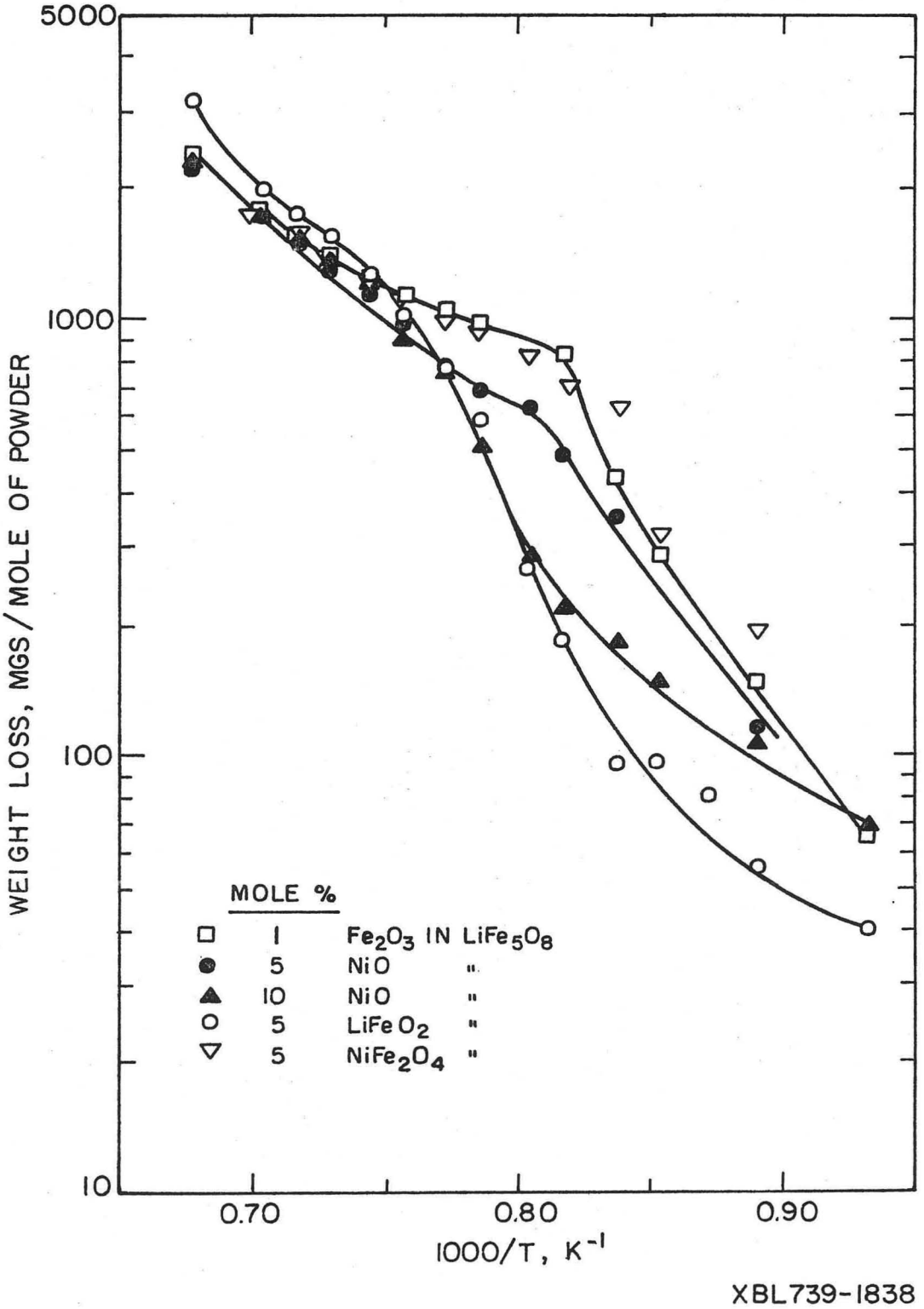

Fig. 26. Equilibrated weight loss data for various compositions. Equilibration was always achieved in air.

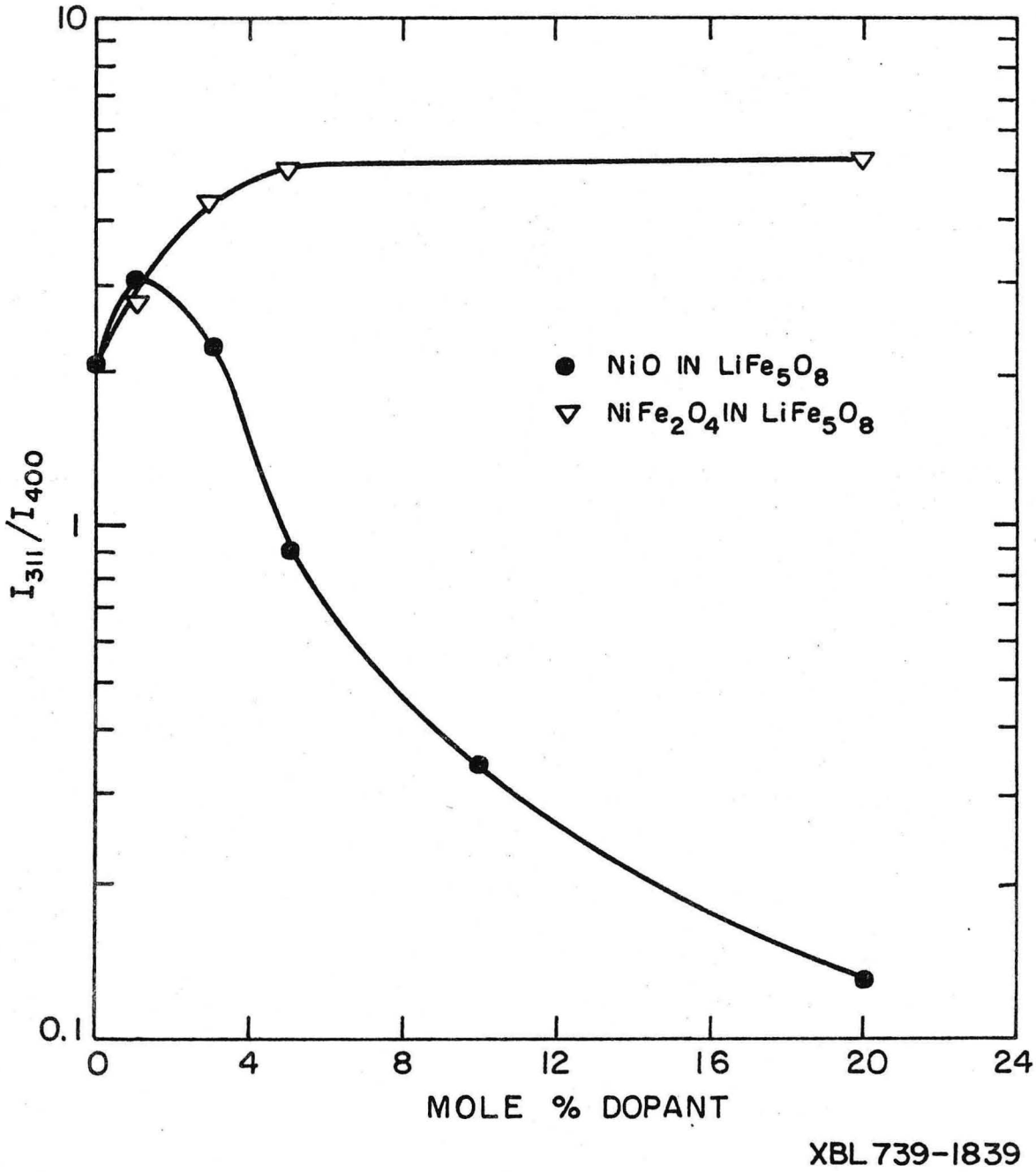

Fig. 27. X-ray data for doped specimens sintered at 1150°C for 2 h in 1 atm O_2 and using stoichiometric packing powder.

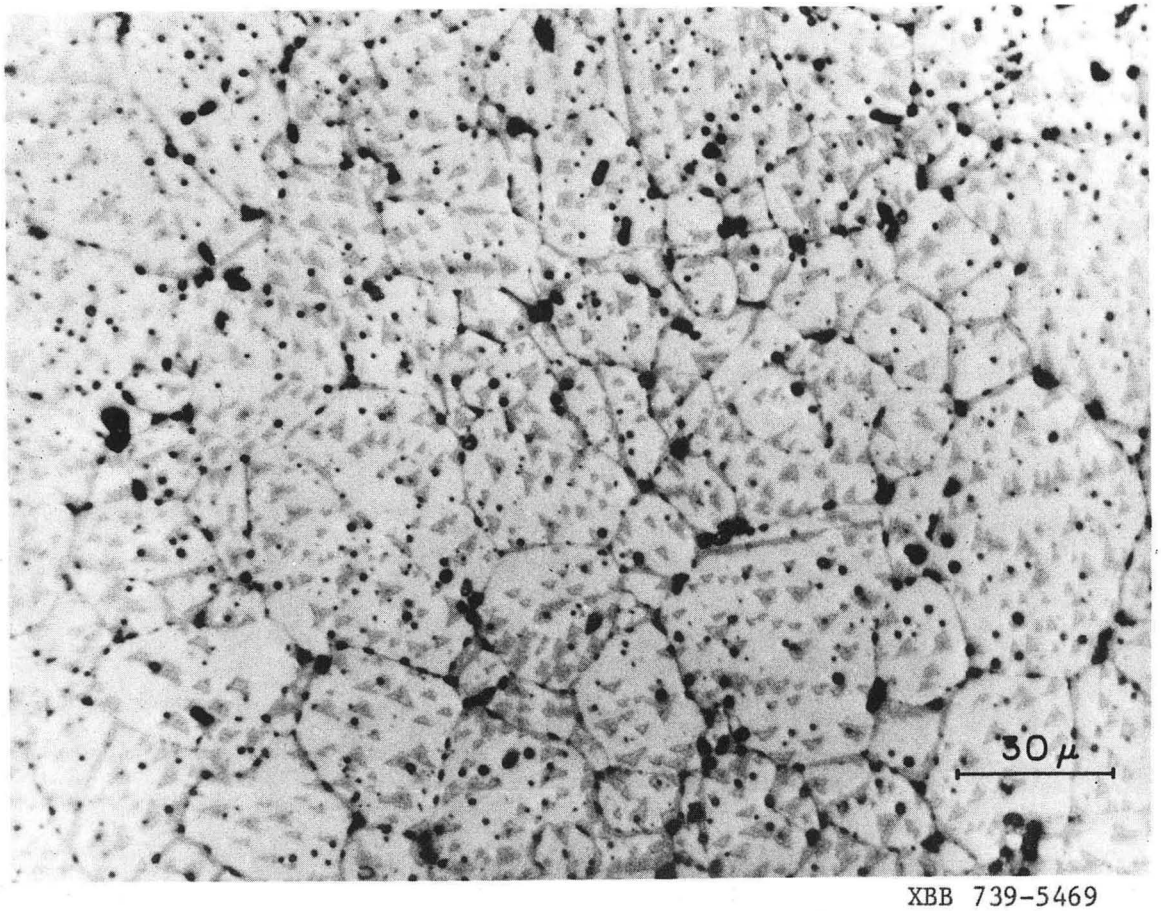

XBB 739-5469

Fig. 28. Microstructure of a specimen of composition ($LiFe_5O_8$ + 3 mol% $LiFeO_2$) sintered at 1150°C for 2 h in 1 atm O_2 and using stoichiometric packing powder.

$NiFe_2O_4$ dopant gives significantly different results than that of a NiO dopant. Microstructural studies revealed uniformly small grains with pores exclusively in the grain corners for all compositions (Fig. 29). This may be due to a slight cation deficiency in the ferrite composition[20] and therefore it can be assumed that the density drop, as has been observed with the addition of $NiFe_2O_4$ (Fig. 23), is due to a retarded densification rate. The cation deficiency may be due to a slight lithia loss or to a slightly cation deficient starting composition which could not be controlled or detected during its preparation. Thermogravimetric data for an equilibrated run with 5 mol% $NiFe_2O_4$ in $LiFe_5O_8$ is shown in Fig. 26. The close correspondence between the data for this composition and for the 1 mol% Fe_2O_3 in $LiFe_5O_8$ indicates the probable cation deficiency in the mixed ferrite composition. X-ray data in Fig. 27, where the I_{311}/I_{400} ratio has also been plotted for $NiFe_2O_4$ containing compositions, shows predominantly a spinel phase on the sintered surfaces of the specimens. This is also indicative of a cation deficiency.

(2) <u>DC Resistivity</u>

In Fig. 30, dc resistivity values for sintered specimens have been plotted against the amount of dopants (NiO or $NiFe_2O_4$). In both cases the resistivity dropped sharply with minute additions of the dopant followed by a rapid increase with increasing amount of the additions. In the case of the NiO dopant, where reaction 14 leads to excess $LiFeO_2$ in the composition, the initial drop in the resistivity value is somewhat surprising. This drop was not observed in $LiFeO_2$ excess compositions sintered under identical conditions (Fig. 19). This discrepancy

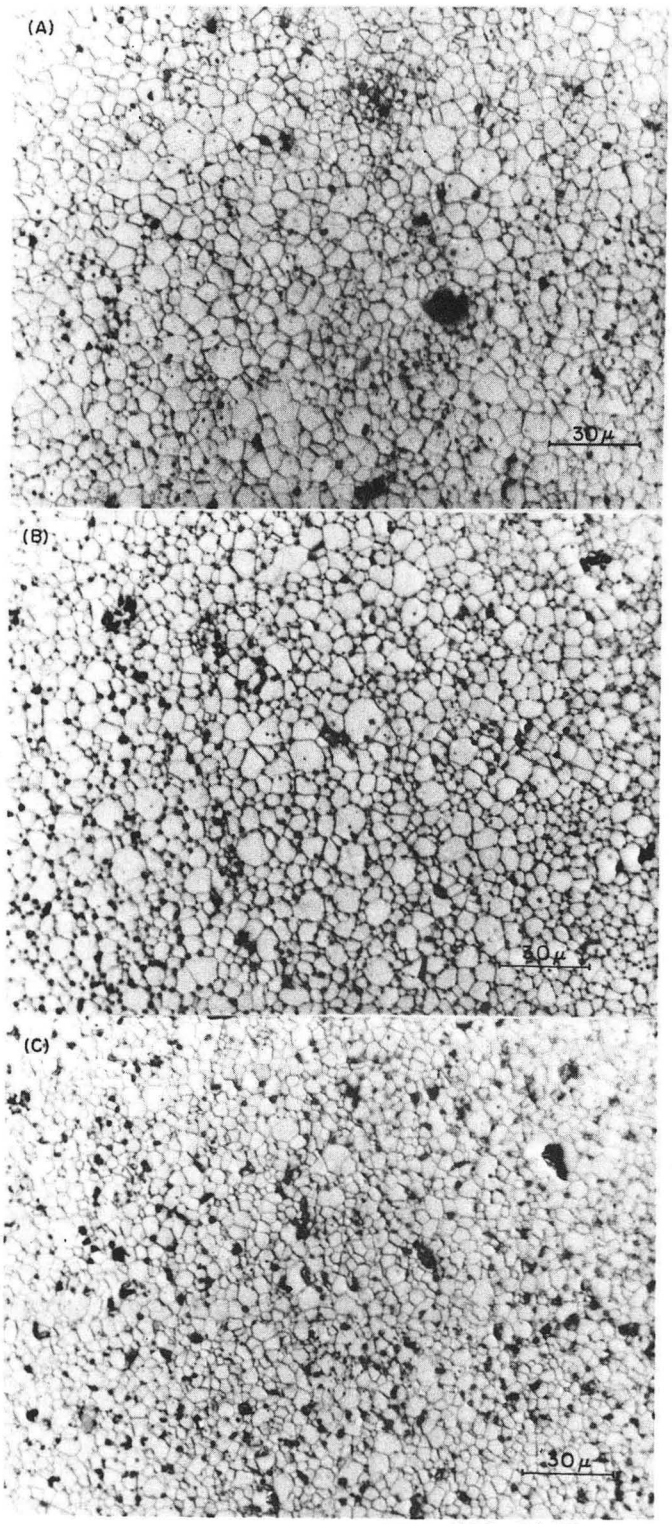

XBB 739-5467

Fig. 29. Influence of $NiFe_2O_4$ dopant on the microstructure of the specimens sintered at 1150°C for 2 h in 1 atm O_2 and using stoichiometric packing powder. (A) 1 mol% $NiFe_2O_4$, (B) 10 mol% $NiFe_2O_4$, (C) 20 mol% $NiFe_2O_4$.

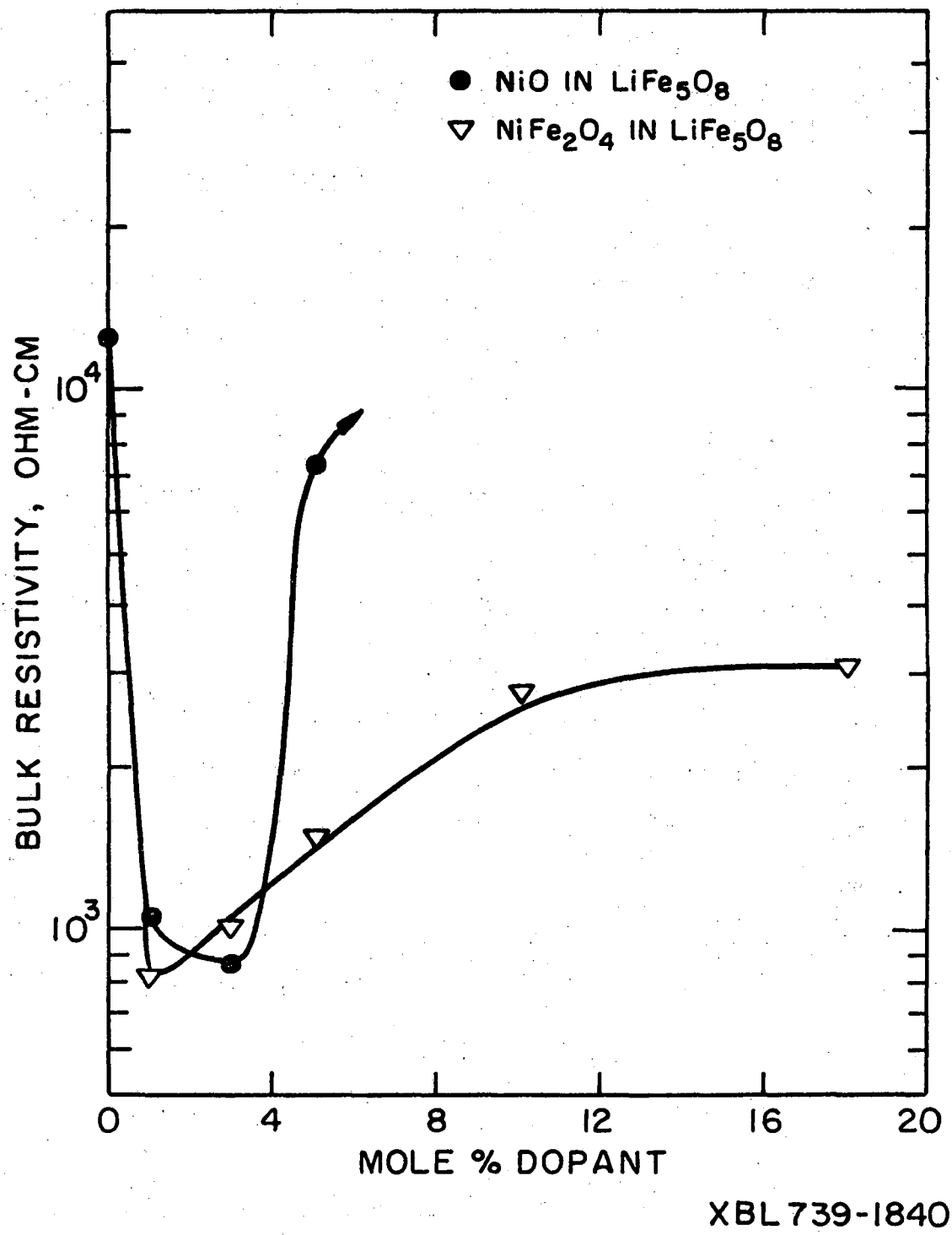

Fig. 30. Influence of dopants on the bulk resistivity of the specimens sintered at 1150°C for 2 h in 1 atm O_2 and using stoichiometric packing powder.

can be accounted for by the assumption that at least part of the NiO dopant (less than or equal to 1 mol% NiO which is equivalent to 0.5 mol% $LiFeO_2$) goes into solid solution with the lithium ferrite composition. This forms excess oxygen vacancies which may act as the current carriers in the anion deficient side.[37,38] Beyond the solubility limit, the resistivity would tend to rise because of the appearance of a second phase. In the previously presented data (Fig. 19) the minimum $LiFeO_2$ content in the lithia rich side (1 mol% $LiFeO_2$) is apparently above the solid solubility limit and therefore no resistivity drop was observed on the anion deficient side.

Another plausible explanation for this resistivity drop could be due to the solution of NiO which destroys the octahedral ordering in lithium ferrite. Since disordered compositions are known[7,38,42] to have a lower resistivity than that of the ordered specimens, this loss of ordering in the composition may lead to a drop of the resistivity value.

Addition of minute amounts of $NiFe_2O_4$ also lowers the resistivity value significantly (Fig. 30). This also may be due to the disordering of the lithium ferrite composition. The subsequent increase in resistivity with further additions of $NiFe_2O_4$ cannot be due to a second phase because secondary phases were not detected in the mixed ferrite compositions. Thus this increase may simply be due to the decrease in density or to nickel ferrite which, in general, has a higher resistivity than that of lithium ferrite.[2]

(3) <u>B-H Loop Parameters</u>

Wijn et al.[3] first reported that the squareness ratio R_s of lithium ferrite can be improved markedly by the addition of Ni^{+2} in the system.

The R_s value for all the specimens in this study was better than 0.85 and with the addition of NiO or $NiFe_2O_4$, slight improvement in the squareness was achieved. In Fig. 31, the coercive force (H_c) has been plotted against the amount of dopant. A NiO addition enhances the grain growth and thus the H_c value dropped significantly with increasing NiO content in the composition. $NiFe_2O_4$ dopant decreases the sinter density and also the grain size was small (in fact, the lower density specimens had a smaller grain size as is evident in Fig. 29) and therefore the value increased with increasing amounts of $NiFe_2O_4$.

Maximum induction values (B_{max}) decreased slightly with NiO or $NiFe_2O_4$ addition.

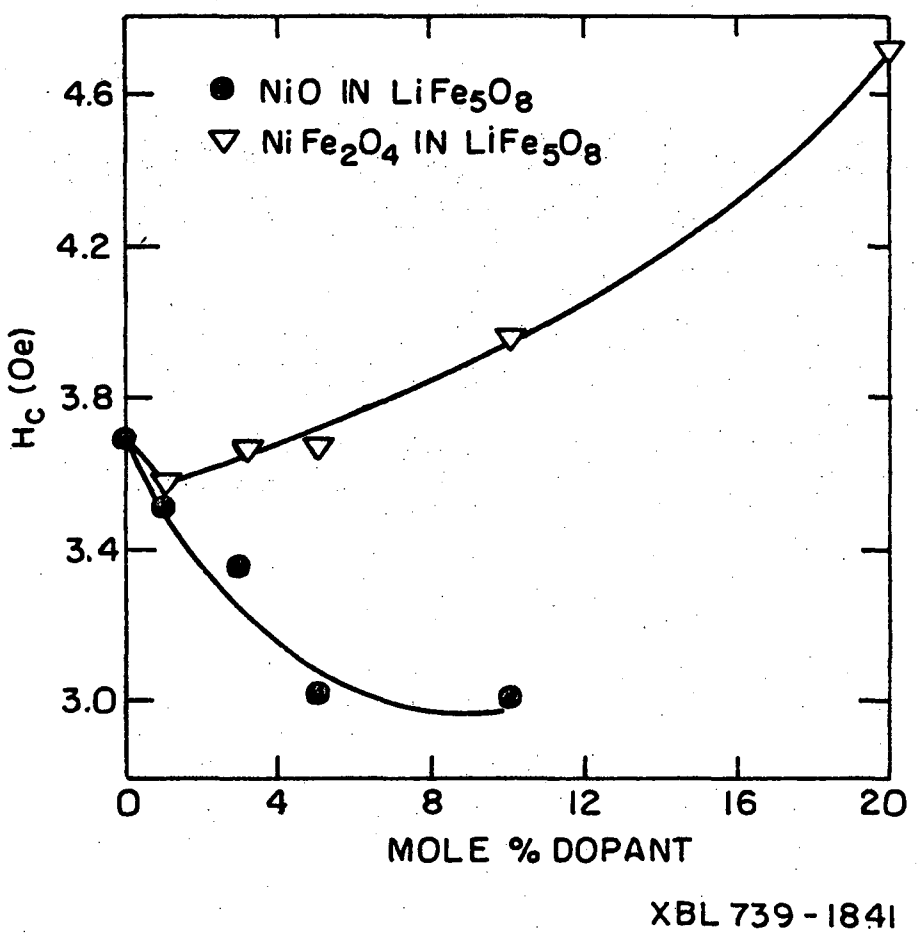

Fig. 31. Influence of dopants on the coercive force (H_c) of the specimens sintered at 1150°C for 2 h in 1 atm O_2 and using stoichiometric packing powder.

V. SUMMARY AND CONCLUSIONS

Lithium ferrite spinel ($LiFe_5O_8$) has attracted considerable attention because of its square loop magnetic properties coupled with the superior temperature stability. Its processing is difficult due to the loss of lithium and oxygen during the sintering process. In this investigation, lithium ferrite and related compositions have been studied to characterize the material loss behavior with heat treatment, and also to determine the influence of sintering parameters, stoichiometry and selected dopants on the densification, microstructure, and electrical and magnetic properties of the sintered material.

Extensive thermogravimetric work in air is reported with compositions which varied widely from the excess lithia side (anion deficient) to the excess Fe_2O_3 region (cation deficient). This data is important because the material loss has a strong influence on the defect structure, which in turn influences the sinterability and most other properties of the sintered ferrite. It has been noted that there is a strong tendency for the composition to adjust itself through weight loss (lithium or oxygen loss as the case may be), and move into the spinel single phase region and then equilibrate with the atmospheric oxygen. Weight loss behavior of nickel ferrite and zinc ferrite compositions has also been studied for comparison purposes. It has been demonstrated that the cation deficient inverse spinel compositions (e.g. Fe_2O_3 excess lithium ferrite or nickel ferrite) exhibit a different behavior than that exhibited by normal (zinc ferrite) or near normal (magnesium ferrite) cation deficient ferrites. The activation energy for the solid-oxygen equilibria in an inverse composition was found to be 32.75 Kcal/mole, whereas

the same for the near normal magnesium ferrite composition was reported to be 22.8 Kcal/mole.

Polycrystalline compacts were sintered using a packing powder technique where the specimens were buried deep into a packing powder atmosphere to control the lithium loss. High oxygen atmosphere was used in the surroundings to control the oxygen loss. The activation energy for the sintering process was found to be 143 ± 15 Kcal/mole. It was observed that the stoichiometry of the starting composition had a pronounced effect on most of the properties that were investigated. Anion deficient compositions led to denser specimens with higher dc resistivity values and squarer B-H loops having low coercive forces. But discontinuous grain growth was favored in these compositions. Also, it was observed that the dc resistivity of these polycrystalline specimens was strongly dependent on the microstructure. It is postulated that the grain boundaries acted as the higher conducting path in these systems. The influence of the packing powder composition on the properties of sintered lithium ferrite was also investigated. The strongest influence was observed on the coercive force value.

Lithium ferrite compacts doped with controlled amounts of NiO or $NiFe_2O_4$ were sintered using a stoichiometric packing powder under one atmosphere oxygen pressure. Both the dopants had only a slight effect on the densification. NiO favored discontinuous grain growth, whereas $NiFe_2O_4$ suppressed it. Experiments were also done relating dc resistivity and B-H loop parameters with the amount of dopants and the results have been discussed in terms of compositional defects and microstructure.

ACKNOWLEDGMENT

I am deeply indebted to Professor R. M. Fulrath for his continuous guidance and support during this work. I would also like to express my sincere appreciation to Drs. James Reed, Alton Lacy and Robert Holman for their comments and suggestions at the early stages of this work. Innumerable discussions with John Sherohman were always useful and were highly appreciated.

Further thanks are extended to the staff of the Inorganic Materials Research Division for their outstanding support throughout this work.

This work was done under the auspices of the U. S. Atomic Energy Commission.

REFERENCES

1. P. B. Braun, Nature, 170, 1123-24 (1952).

2. Handbook of Microwave Ferrite Materials, ed. W. H. Van Anlock, Academic Press, 1965.

3. H. P. J. Wijn, E. W. Gorter, C. J. Esveldt and P. Gelderman, Philips Technical Rev., 16 [2] 45-58 (1954).

4. E. A. Schwabe and D. A. Campbell, J. App. Phys., 34 [4, Pt 2] 1251-53 (1963).

5. R. G. West, J. App. Phys., 34 [4, Pt. 2] 1113-14 (1963).

6. D. B. Rogers, R. W. Germann and R. J. Arnott, J. App. Phys., 36 [8] 2338-42 (1965).

7. R. G. West and A. C. Blankenship, J. Am. Ceram. Soc., 50 [7] 343 (1967).

8. P. K. Baltzer, U. S. Pat. 3,034,987 (1962).

9. D. H. Ridgeley, H. Lessof and J. D. Childress, J. Am. Ceram. Soc., 52 [6] 304-311 (1970).

10. A. J. Pointon and R. C. Saull, J. Am. Ceram. Soc., 52 [3] 157-60 (1969).

11. R. B. Atkin, Ph.D. Thesis at the University of California, Berkeley, 1970.

12. P. Reinjnen, Reactivity of Solids, G. M. Schwab, ed., (Elsevier Pub. Co., Amsterdam, 1965), pp 562-71.

13. P. Reinjnen, Philips Res. Rep., 23, 151-88 (1968).

14. P. Reinjnen, Philips Tech. Rev., 31 [1] 24-30 (1970).

15. D. W. Strickler and R. Roy, J. Am. Ceram. Soc., 44 [5] 225-30 (1961).

16. Ceramic Processing, Materials Advisory Board, National Academy of Sciences, Washington, D.C., Publication 1576, 1968.

17. R. L. Coble, J. App. Phys., 32 [5] 787-92 (1961); ibid, pp. 793-99.

18. A. L. Stuijts, Proc. Brit. Ceram. Soc., 2, 73-81 (1964).

19. A. L. Stuijts, Ceramic Microstructure, R. M. Fulrath and J. A. Pask, eds., (John Wiley and Sons, New York, 1968), pp 443-74.

20. P. Reinjnen, Science of Ceramics, 4, 169-88 (1968).

21. P. Reinjnen, Reaction of Solids, J. W. Mitchell, R. C. Devries, R. W. Roberts and P. Cannon, eds., (John Wiley and Sons, New York, 1969), pp 99-114.

22. P. Reinjnen, Problems of Nonstoichiometry, A. Rabenau, ed., (North Holland Publishing Co., Amsterdam, 1970), pp. 219-38.

23. D. W. Readey, J. Am. Ceram. Soc., 49 [7] 366-369 (1966).

24. A. L. Stuijts, Ferrites: Proceedings of the International Conference, Y. Hoshino, S. Iida and M. Sugimoto, eds., (University of Tokyo Press, 1971), pp. 108-13.

25. A. M. Lacy, Unpublished work at the University of California, Berkeley, 1970.

26. C. F. Jefferson, Tech. Rep. No. 7, College of Engineering, The University of Michigan, 1959.

27. Yu. D. Tretyakov, N. N. Oleynikov, Yu. G. Metlin and A. P. Erastova, J. Solid State Chem., 5, 191-99 (1972).

28. O. N. Salmon and L. Marcus, J. Am. Ceram. Soc., 43 [10] 549-550 (1960).

29. D. Adler, Chap. 2 in Physics of Electronic Ceramics: Part A., L. L. Hench and D. B. Dove, eds., (Marcel Dekker, Inc., New York, 1971).

30. I. Bransky and N. M. Tallan, Chap. 3 in Physics of Electronic Ceramics: Part A, L. L. Hench and D. B. Dove, eds., (Marcel Dekker, Inc., New York, 1971).

31. A. J. Bosman and H. J. van Daat, Adv. in Physics, 19, 1-117, 1970.

32. Conduction in Low Mobility Materials: Proceedings of the Second International Conference, N. Klein, D. S. Tanhauser and M. Pollak, eds., (Taylor and Francis Ltd., London, 1971).

33. D. Adler, Bull. Am. Ceram. Soc., 52 [2] 154-59 (1973).

34. N. F. Mott, Phil. Mag., 6 [62] 287-309 (1961).

35. Introduction to Solid State Physics, Fourth Edition by C. Kittel (John Wiley and Sons, New York), p. 389.

36. I. G. Austin and N. F. Mott, Adv. Phys., 18, 41-102 (1969).

37. F. F. Y. Wang, R. L. Gravel and M. Kestigian, J. App. Phys., 48 [3] 1131-32 (1967).

38. F. F. Y. Wang, R. L. Gravel and M. Kestigian, IEEE Trans. on Mag., MAG-4 [1] 55-58 (1968).

39. D. Elwell and D. S. Tanhauser, Solid State Comm., 8, 179-81 (1970).

40. L. G. Van Uiter, J. Chem. Phys., 23 [10] 1883-87 (1955).

41. G. H. Jonker, J. Phys. Chem. Solids, 9, 165-75 (1959).

42. E. Kato, Bull. Chem. Soc. Japan, 31 [1] 113-117 (1958).

43. G. Bandyopadhyay, A. M. Lacy and R. M. Fulrath, Submitted to the J. Am. Ceram. Soc.

44. H. Lessoff and J. D. Childress, J. App. Phys., 38 [9] 3455-57 (1967).

LEGAL NOTICE

This report was prepared as an account of work sponsored by the United States Government. Neither the United States nor the United States Atomic Energy Commission, nor any of their employees, nor any of their contractors, subcontractors, or their employees, makes any warranty, express or implied, or assumes any legal liability or responsibility for the accuracy, completeness or usefulness of any information, apparatus, product or process disclosed, or represents that its use would not infringe privately owned rights.

TECHNICAL INFORMATION DIVISION
LAWRENCE BERKELEY LABORATORY
UNIVERSITY OF CALIFORNIA
BERKELEY, CALIFORNIA 94720